CHAPTER 5

RESULTS AND DISCUSSION

5.1 Introduction:

Predictions of pump performance are almost a daily practice for the pump manufacturers in quoting solutions to pumping problems. These predictions often become commercially guaranteed conditions, which have to be demonstrated by testing and can, hold the designer in anticipation until the actual performance is known.

The theoretical approach; which has been presented in *chapter 3*, is applied for an End Suction pump model of single stage with rectangular volute casing type. The geometric parameters of this pump are listed in table (4-1) chapter 4. The numerical modeling by CFD and experimental results are presented in present chapter.

The results of the experimental investigation are presented and discussed for different impeller configurations as mentioned in table 4-2 at four different running speeds (1750, 2000, 2500 and 2900 RPM.). The main object of these tests is to indicate the effect of different shorted blade position on pump performance.

The standard impeller (configuration A) has the same geometric and hydraulic parameters of the pump model that is used in the theoretical approach. Experimental results are represented and explained using the detail numerical results of velocities and pressure. Therefore; this chapter can be classified into:

i) Theoretical results using CFD;

ii) Experimental results;

5.2 Theoretical results using CFD:

The use of CFD-tools to analyse the flow field in turbo machines and to predict performance parameters has gained enormous popularity in recent years.

In the present study, flow analysis is done on five impellers used in the experimental work. We analyse the extent to which the CFD-methods, typically available in the Fluent commercial package, can be used for the prediction of the head as function of flow rate for constant rotational speed.

A hybrid mesh is created using FLUENT's pre-processor GAMBIT. First, the impeller is generated. One impeller channel is meshed and is then rotationally copied the necessary number of times. The impeller is completely three-dimensional. The mesh is made in a completely unstructured way, mainly using tetrahedral, but other cell forms like pyramids, hexahedra and wedges also occur. The total numbers of calculation nodes are about 40000 nodes for each case. Fig. 5-1 shows views of geometry of all impellers used.

The equations solved are the three-dimensional Reynolds-averaged Navier-Stokes equations. The fluid is incompressible. The segregated solver with implicit formulation is used. As a turbulence model, the Renormalization-Group (RNG) k-€ model is used with non-equilibrium wall functions.

The inlet velocity and the flow direction normal to the boundary are imposed at the inlet. The turbulence intensity is taken as 2%. Flow parameters like pressure and flow rates at the outlet, are extrapolated from the interior.

The present theoretical results of pump at rated flow rate and speed show the followings for all impeller configurations:

- Static pressure distribution.
- Absolute velocity distribution.
- Tangential velocity distribution
- Radial velocity distribution
- Relative velocity distribution
- Flow path line

For the static pressure (Fig. 5-2); it is noticed that the static pressure increases from suction to discharge sides. Pressure at pressure side is much higher than suction side. Better pressure distribution is performed at impeller exit for both impeller configuration B & E. Higher pressure value at exit for impeller configuration B and D respectively compared to impeller configuration A.

For the absolute velocity (Fig. 5-3) and tangential velocity (Fig. 5-4); velocities are increased at impeller exits for configurations B, C, D and E, and absolute velocity distribution became more uniform for impeller B and E.

For the radial velocity (Fig. 5-5); a reduction in radial velocity occurs at the leading edge for all shorted blades**.** Also impeller E shows the best uniformity at exit.

For the relative velocity (Fig. 5-6); Velocity value as pressure side is much higher than in suction side. Uniformity for relative velocity is noticed at exit for impeller configuration B, D and E. Higher velocity value at exit for impeller configuration B and E respectively.

The path lines shown in (Fig. 5-7); as compared to impeller A; indicates reduction in flow circulation for impeller B, D and E respectively comparing to impeller A.

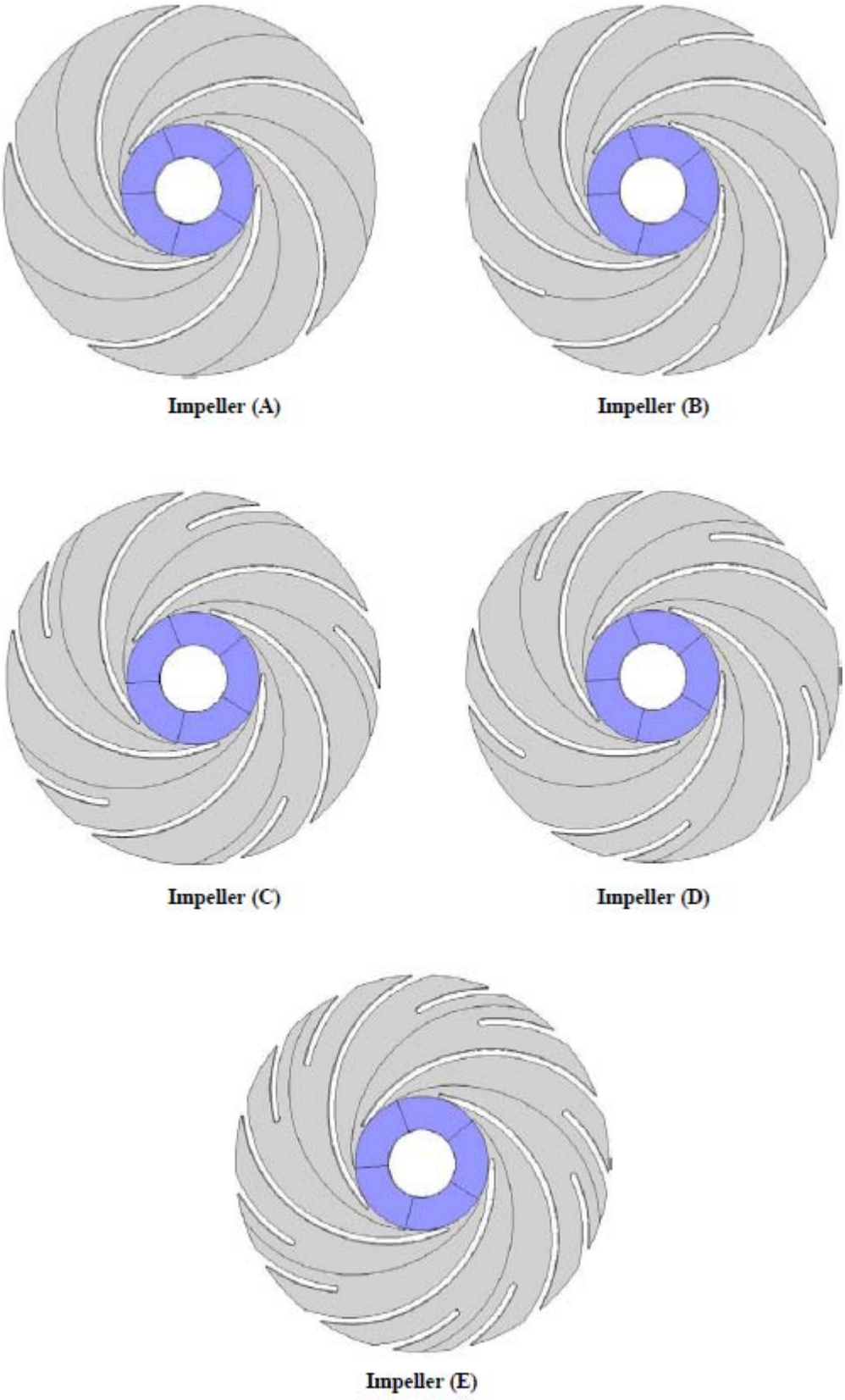

Fig. 5-1 Geometry for all impeller configurations

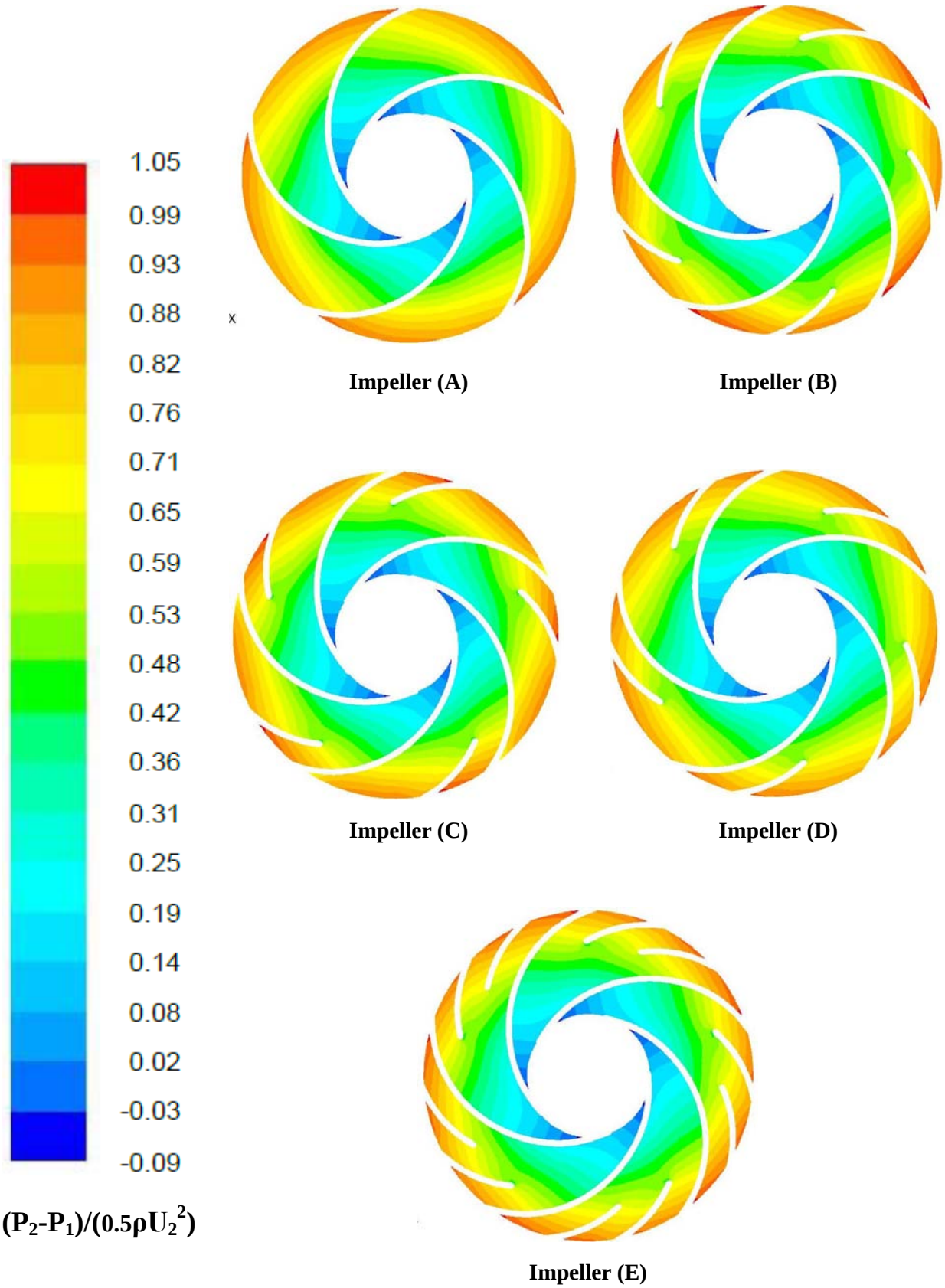

Fig. 5-2 Static pressure distribution for all impellers configurations

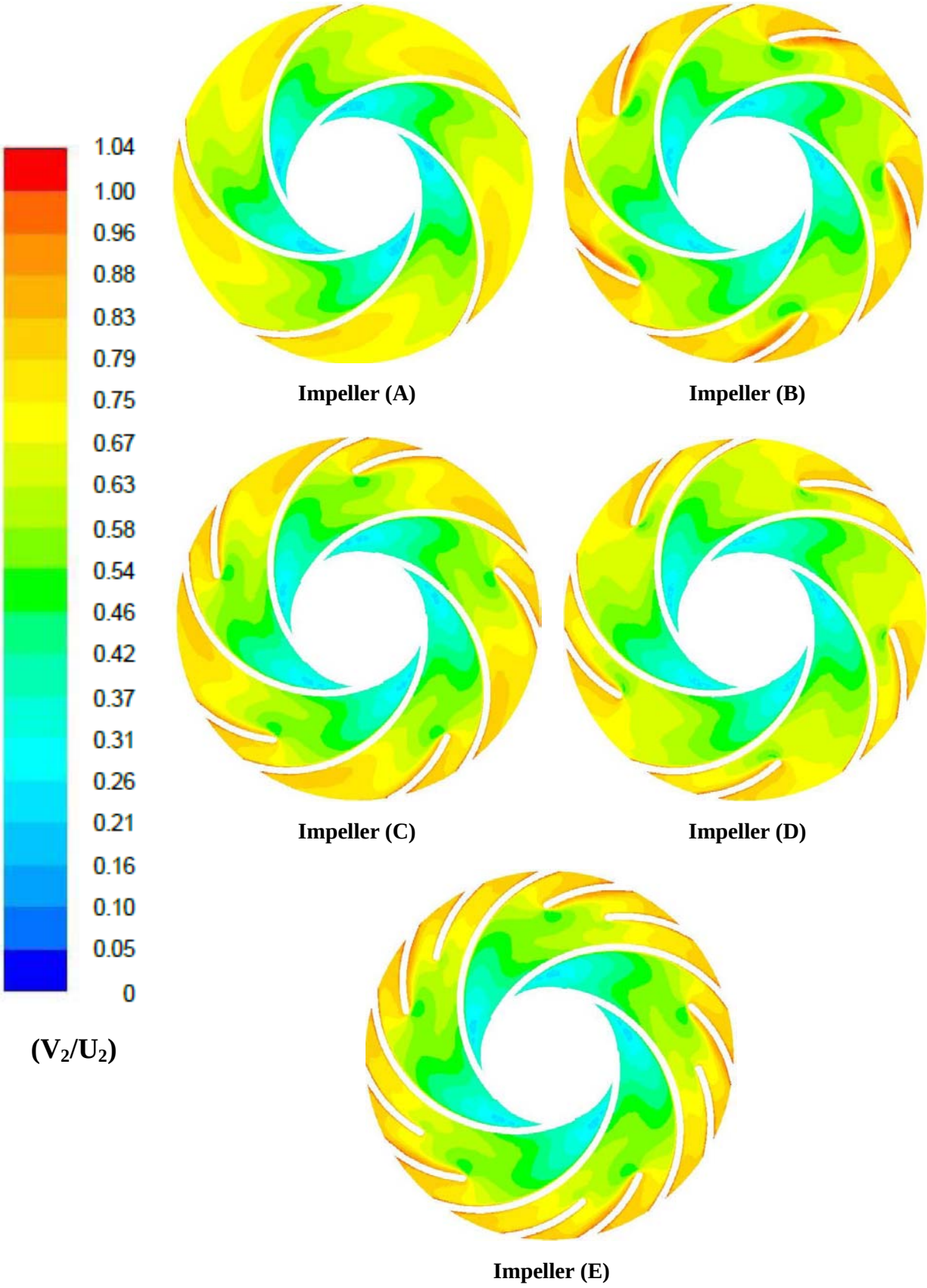

Fig. 5-3 Absolute velocity distribution for all impellers configurations

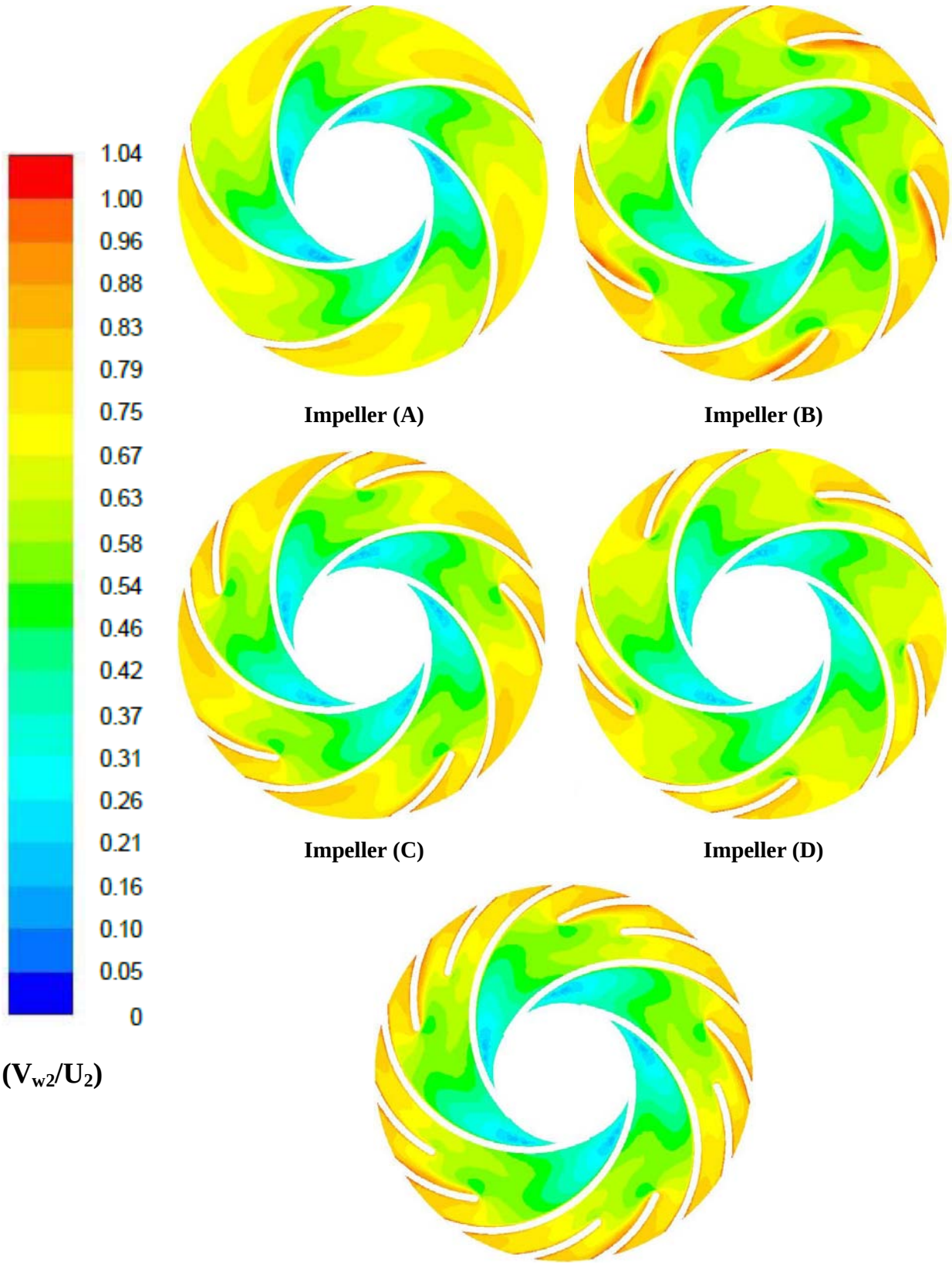

Fig. 5-4 Tangential velocity distribution for all impellers configurations

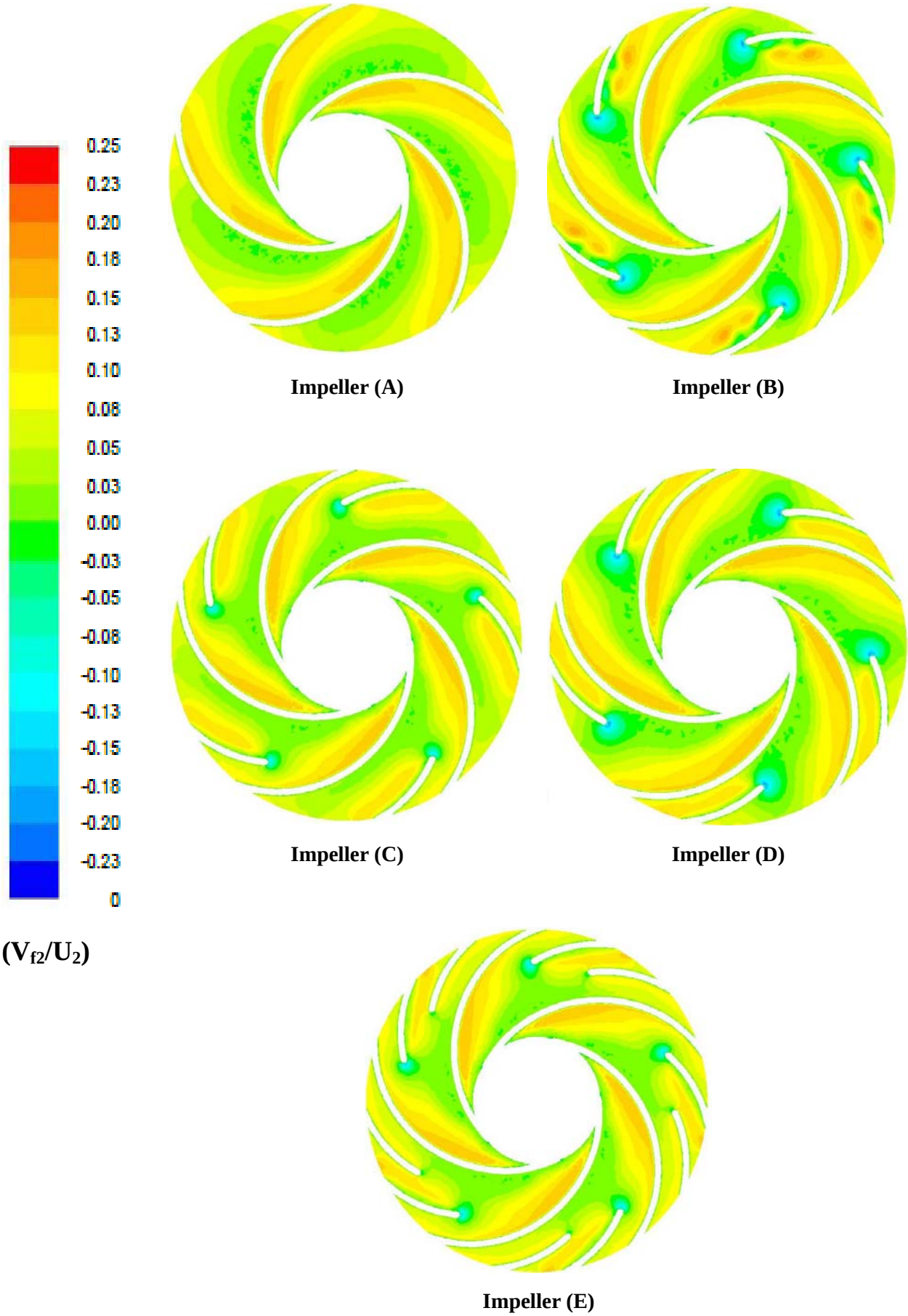

Fig. 5-5 Radial velocity distribution for all impellers configurations

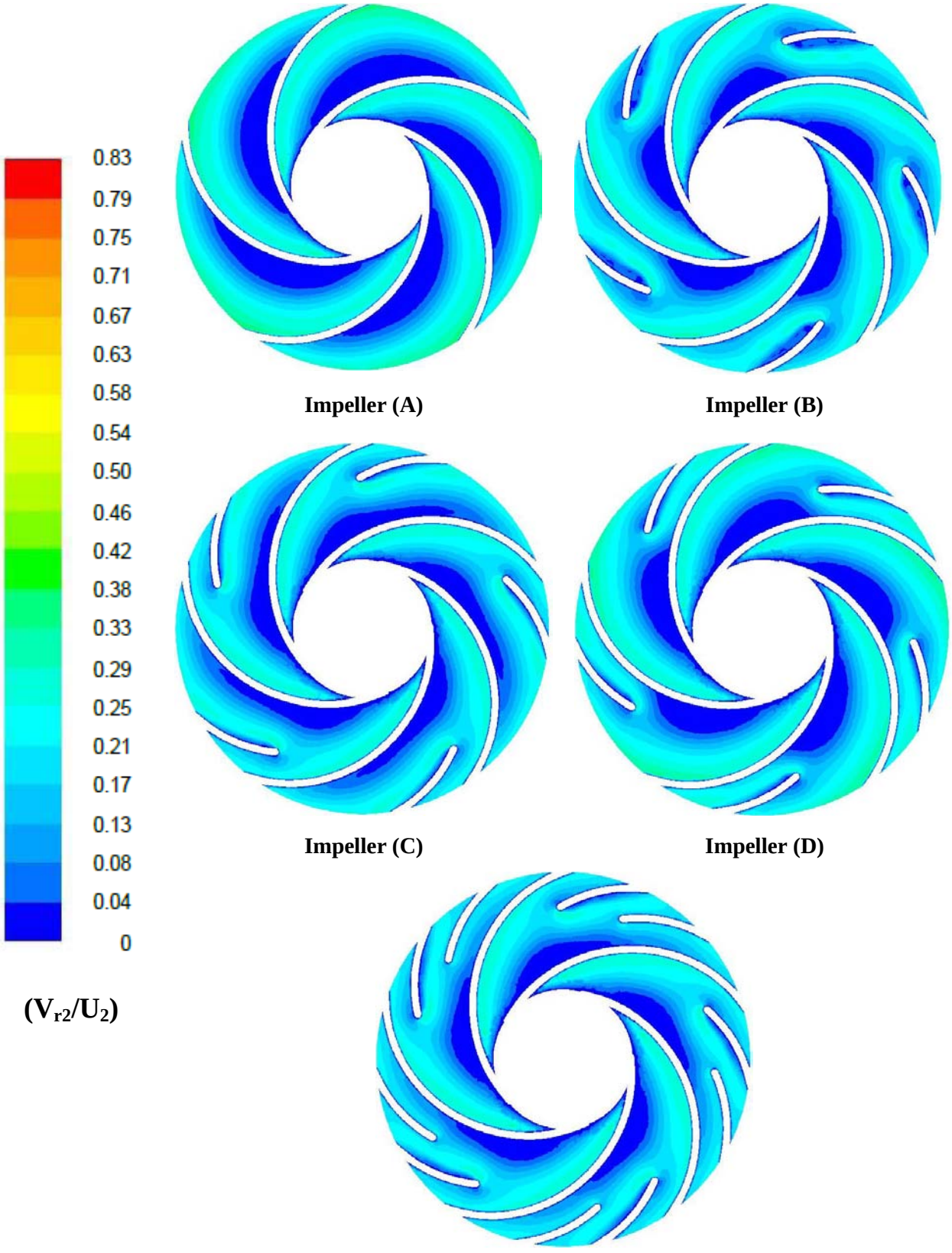

Fig. 5-6 Relative velocity distribution for all impellers configurations

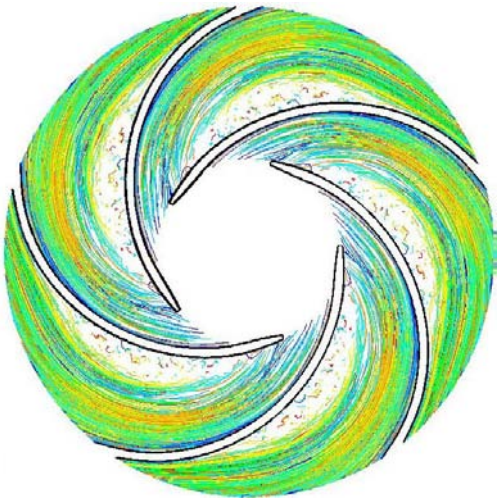

Impeller (A)

Impeller (B)

Impeller (C)

Impeller (D)

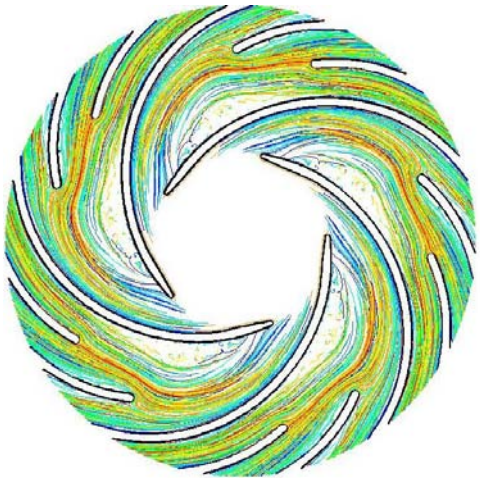

Impeller (E)

Fig. 5-7 Flow path line for all impellers configurations

5.3 Experimental results:

The experimental results of the centrifugal pump performance measurements with standard impeller and different shorted blades impellers are presented at different speeds. The results are plotted in dimensional form for all impeller configurations as (H-Q), (P_{sh}-Q), (η-Q) curves in figures 5-8, 5-10, 5-12, 5-14 and 5-16, and in dimensionless coefficient in figures 5-9, 5-11, 5-13, 5-15 and 5-17.

5.3.1 Performance of the standard impeller (A):

The characteristics curves of the standard impeller at different rotational speeds of 1750, 2000, 2500 and 2900 RPM are shown in dimensional form in figure 5-8, and in dimensionless form in figure 5-9.

The head-flow characteristics curves at different rotational speeds have the normal characteristics for centrifugal pump with smooth trend over the entire range of flow rate without discontinuities.

The efficiency curves show the optimum values of 39.48% at 1750 rpm, 42.47% at 2000 rpm, 39.5% at 2500 rpm and 38.8% at 2900 rpm.

There is nearly complete similarity for the characteristic curves at different speeds, except little scatters are shown at low flow coefficients.

5.3.2 Effect of shorted blade position on pump performance:

The head – flow rate curves given in (figure 5-18) shows that, all impeller configurations from B to E (in dimensional form) have similar trend as the standard impeller (A), except for configurations B and D, the head curves become more flatten (or less steep). The impeller configuration B has a remarkable increase in the pump head as compared with the standard impeller head curve. Also impeller D shows an increase in pump head more than impeller A and less than impeller B. Configurations C shows lower head curves than the standard configuration (A) while impeller E has almost the same head curve of impeller configuration A.

In the power – flow rate curves (figure 5-18), it is observed that, variation of shorted blade position has a slightly effect on the absorbed power and all curves are nearly collapse into a nearly single curve.

In the efficiency – flow rate curves (figure 5-18), it is observed that; at low flow rates the efficiency curves for different impeller configurations A to E have small variations and they are approximately coincident. As flow rate increases these variations in efficiency values increases, but all the curves still have similar trend. In general the flow rate corresponding to peak efficiency occurs for all the impeller configurations at almost the same flow rate (around 12 m^3/hr) except for impeller B which is at higher value of about 14 m^3/hr.

Impeller configurations B, C, D and E show improvement in efficiency at BEP comparing to impeller (A).

The highest value of efficiency is at impeller B (50.63%), D (45.46%), E (44.5%) and C (39.9) respectively; while for impeller A, it is (38.8%).

Experimental results at other speeds (2500, 2000 and 1750 rpm) illustrated dimensionally in figures 5-20, 5-22 and 5-24 and in dimensionless form in figures 5-19, 5-21, 5-23 and 5-25. The results show the same as for 2900 rpm where the efficiency improved for shorted blades impeller configurations B, D, E and C respectively.

Finally, it can be concluded that impeller configuration B (Mid way) has the best improvement in efficiency by 30% from the standard impeller A at best efficiency point at 2900 rpm, 20% at 2500 rpm, 15% at 2000 rpm and 30% at 1750 rpm.

Also, impeller D has improvement in efficiency by 17% from the standard impeller A at best efficiency point at 2900 rpm, 16% at 2500 rpm, 15% at 2000 rpm and 22% at 1750 rpm.

The above performance behaviour is explained by the following analysis:

i) The distortion of the exit velocity profile from the impeller takes place near the suction side of the impeller blade and consequently reduces theoretical head and pump efficiency. This is a result of the diffusion passage of centrifugal impeller, under the effect of adverse pressure gradient, and the side wall boundary layers increase gradually from inlet to outlet, causing the secondary flow under the combined effect of centrifugal and Coriolis forces. This result is gathering of lower energy fluid from pressure side boundary layers to the suction one.

ii) By using a shorted blade, the secondary flow can be prevented effectively from generating and developing. As a result, the flow passage of shorted blades and diffusion angle is small, which will reduce the secondary flow, Therefore an improvement in the pump performance can be achieved by using the shorted blade.

iii) For standard impeller configuration A, there is circulation established between each two blades with radius r, according to Stodola's theory [Yahya] where,

$r = (\pi R_2 \sin\beta_2)/z)$

And the slip factor is given by;

$\delta = 1 - (\pi/z)(\sin\beta_2/(1-\varphi_2 \cot\beta_2)$

For shorted blade impeller configurations B and D with shorted blade, the circulation divided into two small circulations each of radius r smaller than of impeller A because of higher number of blades which increase the slip factor and consequently theoretical head developed by the impeller is improved.

iv) Moreover, the existing of shorted blades provided a better exit flow velocity distribution that can reduce the mixing losses between impeller outlet and volute casing inlet. The cause of improvements in performance of impeller B than D results rather than impeller C is that the circulation intensity near the suction side is less than the pressure side; accordingly the shorted baled in pressure side and mid way has a great effect in reducing this circulation.

v) Furthermore, the increase of pump efficiency of impeller B rather than D can be explained as follow:

The area between the pressure side for the shorted blade and the suction side of the main blade has a great effect on development of impeller performance. On Impeller configuration D this area is larger than in impeller configuration B, this leads to establishment of circulation in bigger size for impeller D rather than B, accordingly the development in pump performance of impeller B is much higher than for impeller D. This is matching the results of numerical model where the highest increase in static pressure is for impeller configurations B and D respectively.

vi) For impeller configuration C, the position of the shorted blade does not affect establishment for the circulation, this is because the circulation is mainly performed near the pressure side of the blade. This is clearly explained why there is no development in pump performance for impeller C, even the performance is much lower than the standard impeller A because the shorted blade is obstructing the flow at exit.

vii) For impeller configuration E, the numerical results shows better static pressure distribution while the experimental results shows lower performance than impeller B and D. Due to the increase of surface are at exit, the friction losses increases, accordingly the overall performance does not improve rather than B and D.

The effect of shorted blade position on the performance of centrifugal impellers at 2900, 2500, 2000 and 1750 rpm are presented non-dimensionally in figures 5-11, 5-13, 5-15 and 5-17 for impeller configurations B, C, D and E. The figures show scatters around similarity curve, this is because inserting of shorted blade between each two complete blades can be considered as geometry change, which consequently produces considerable deviation from the affinity laws.

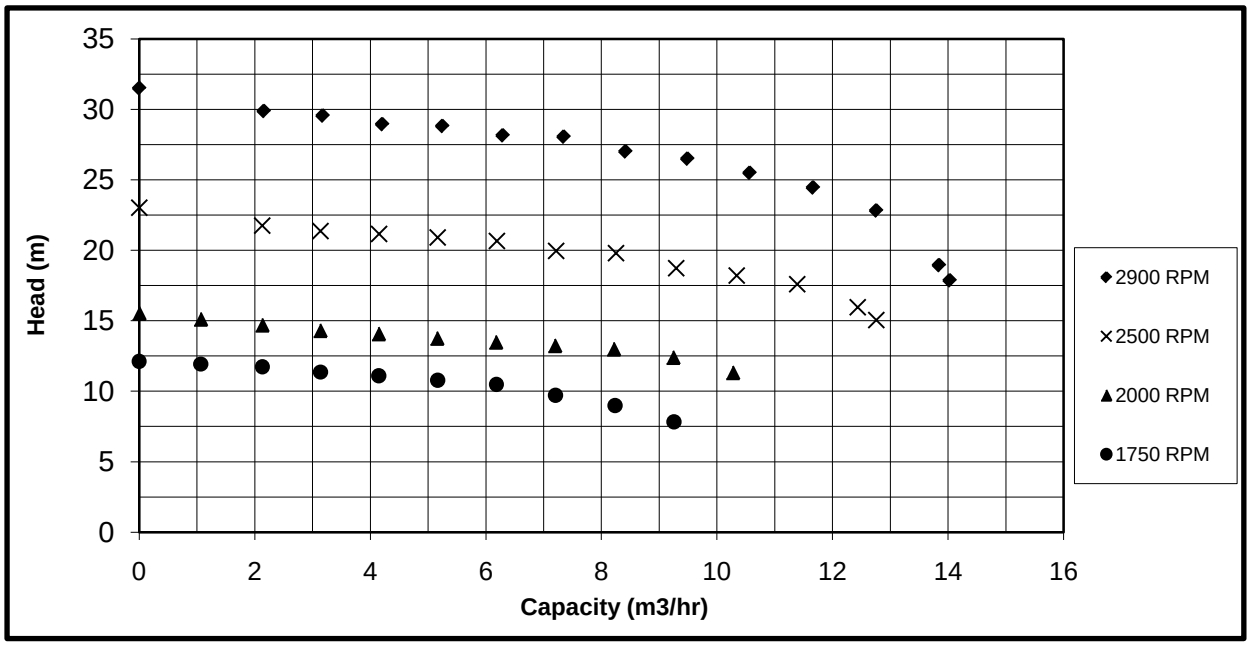

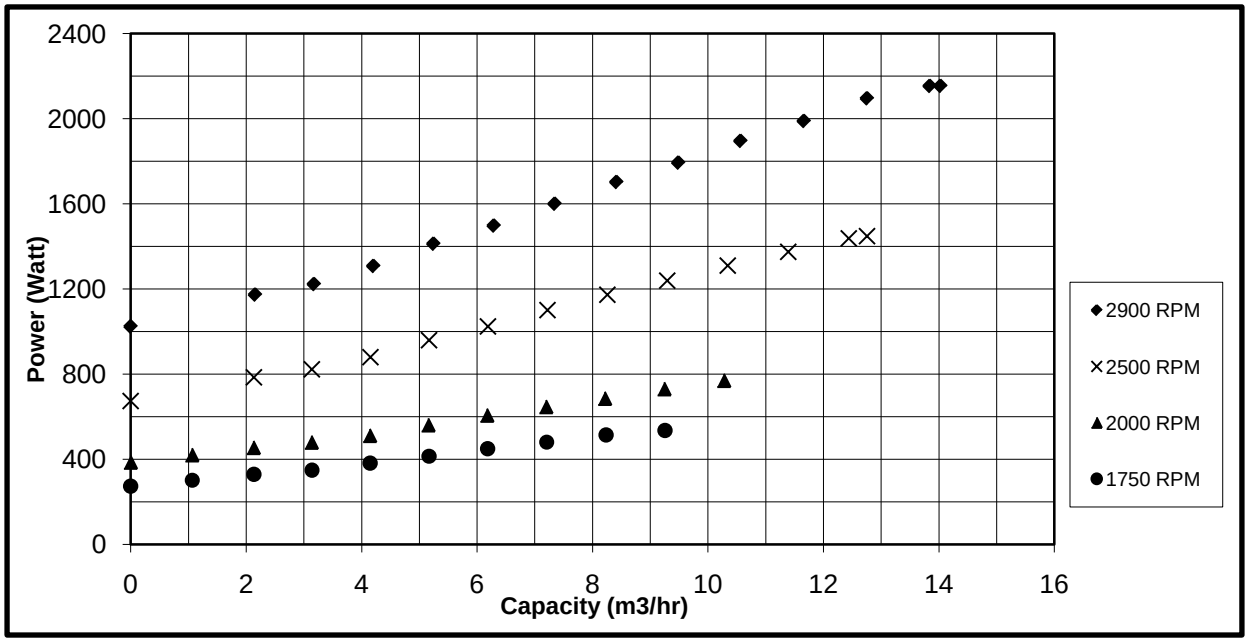

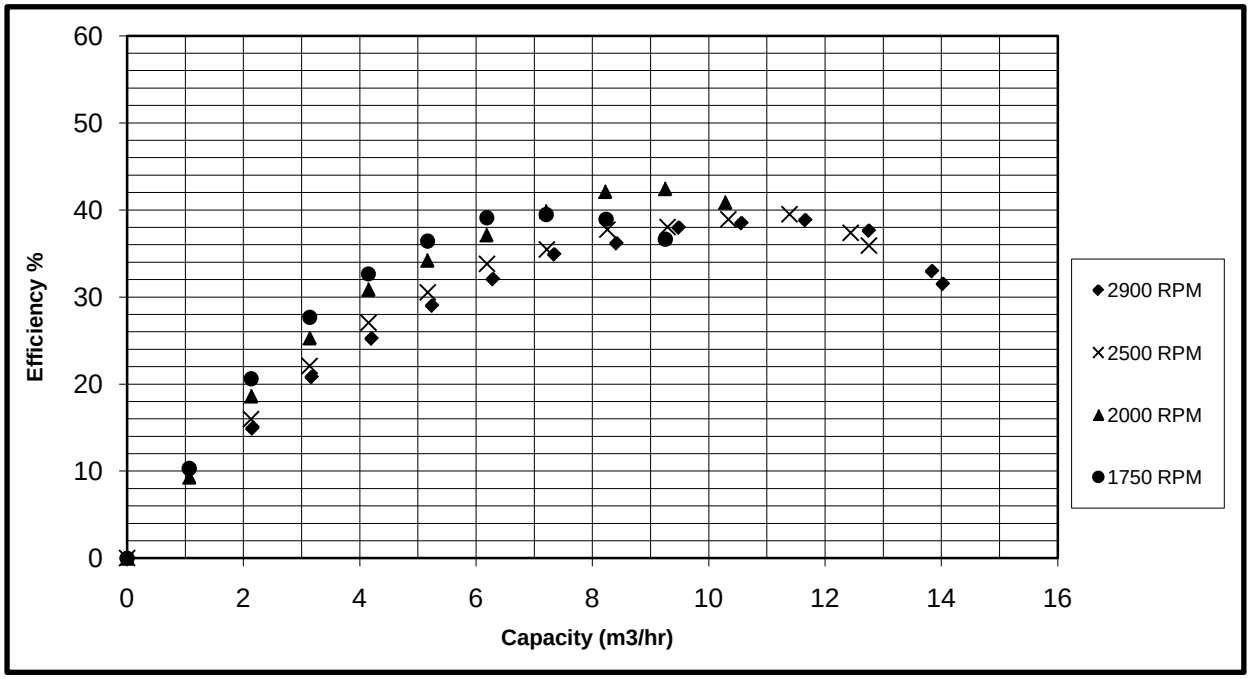

Figure (5-8) Experimental Pump performance for impeller configuration A at different RPM

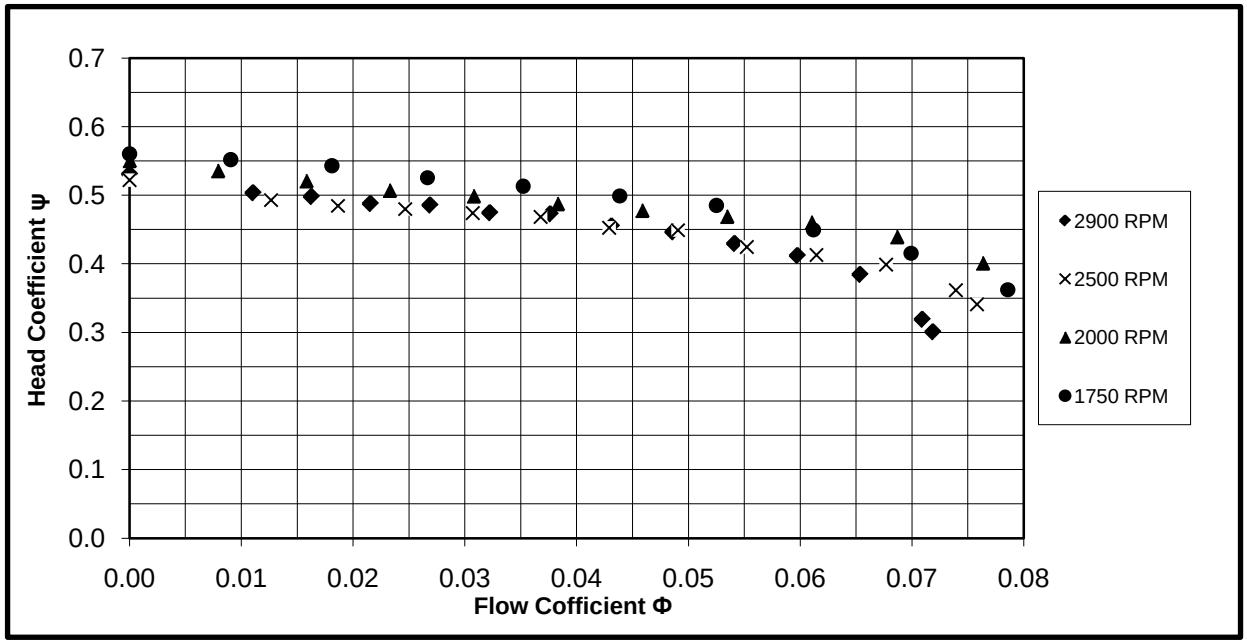

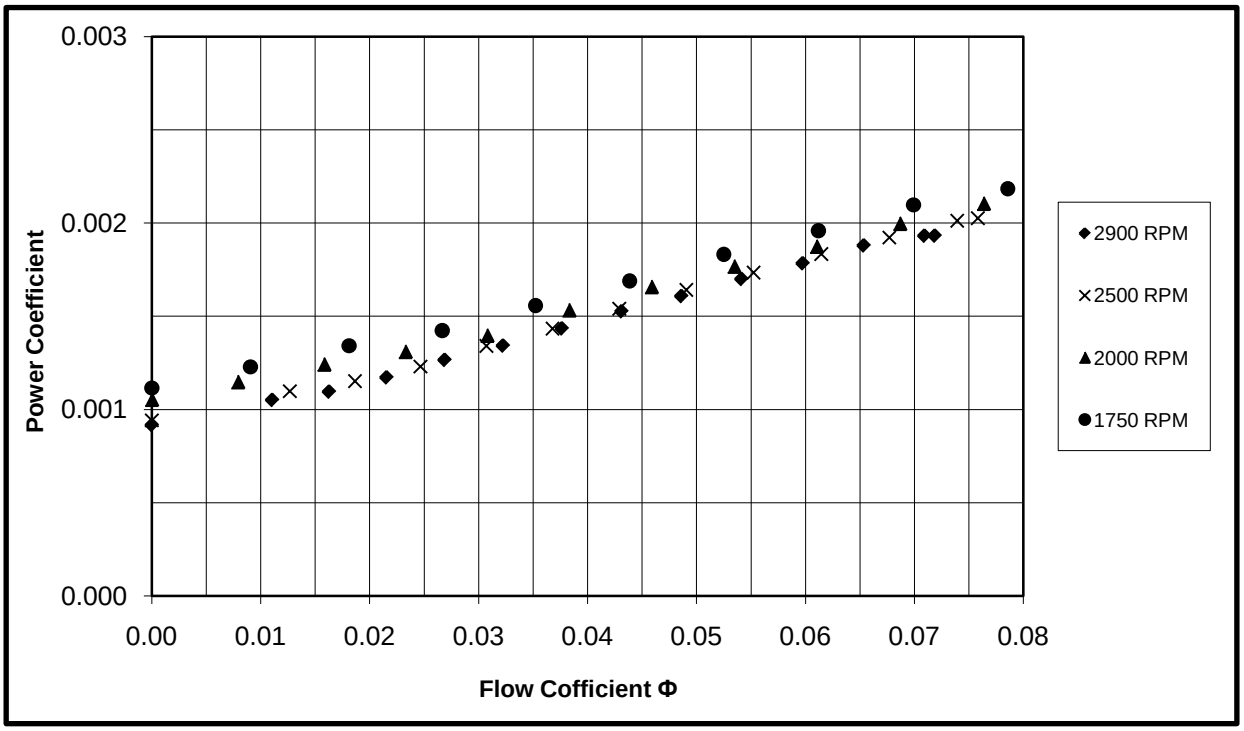

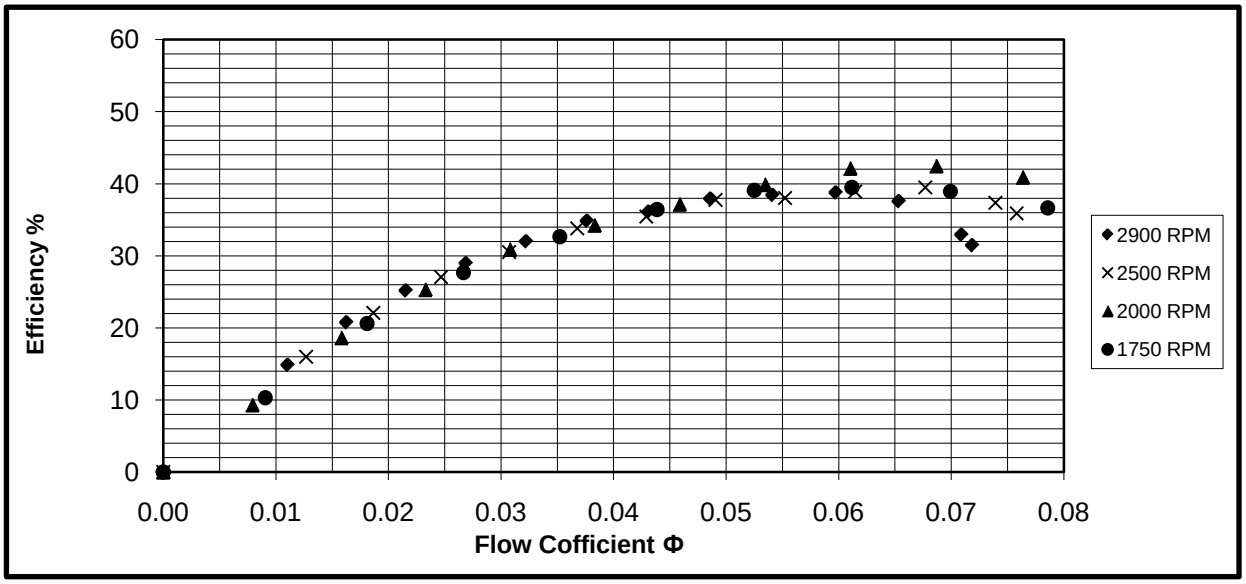

Figure (5-9) Experimental Dimensionless coefficients for impeller configuration A at different RPM

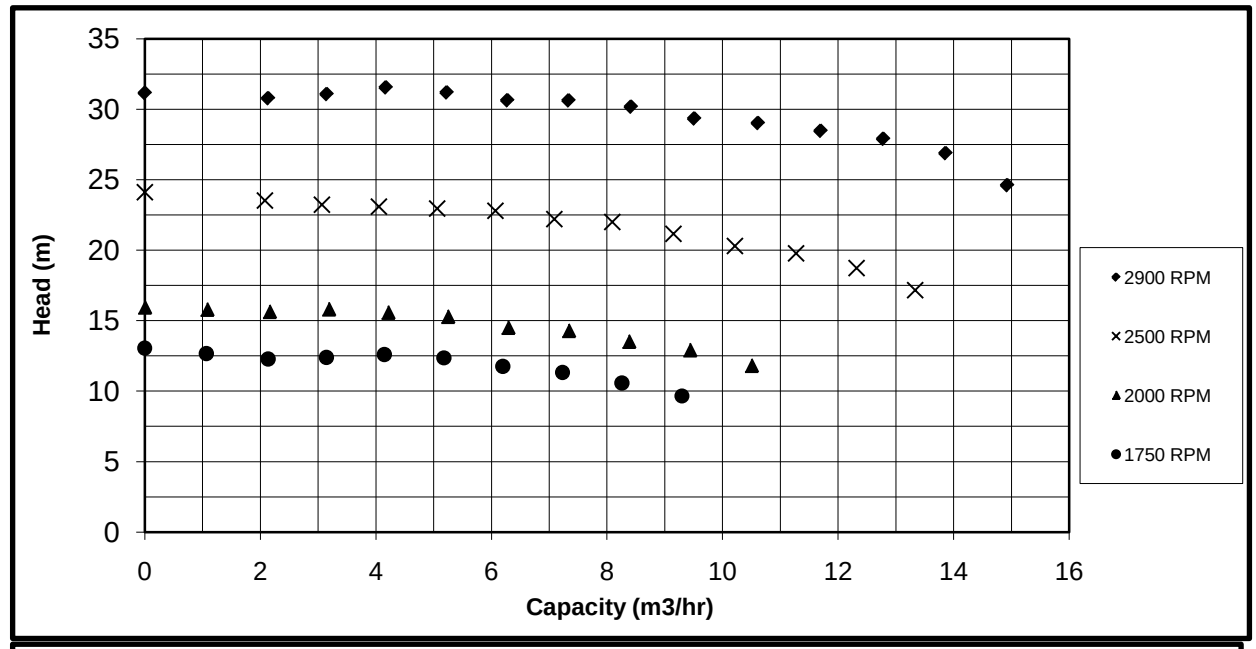

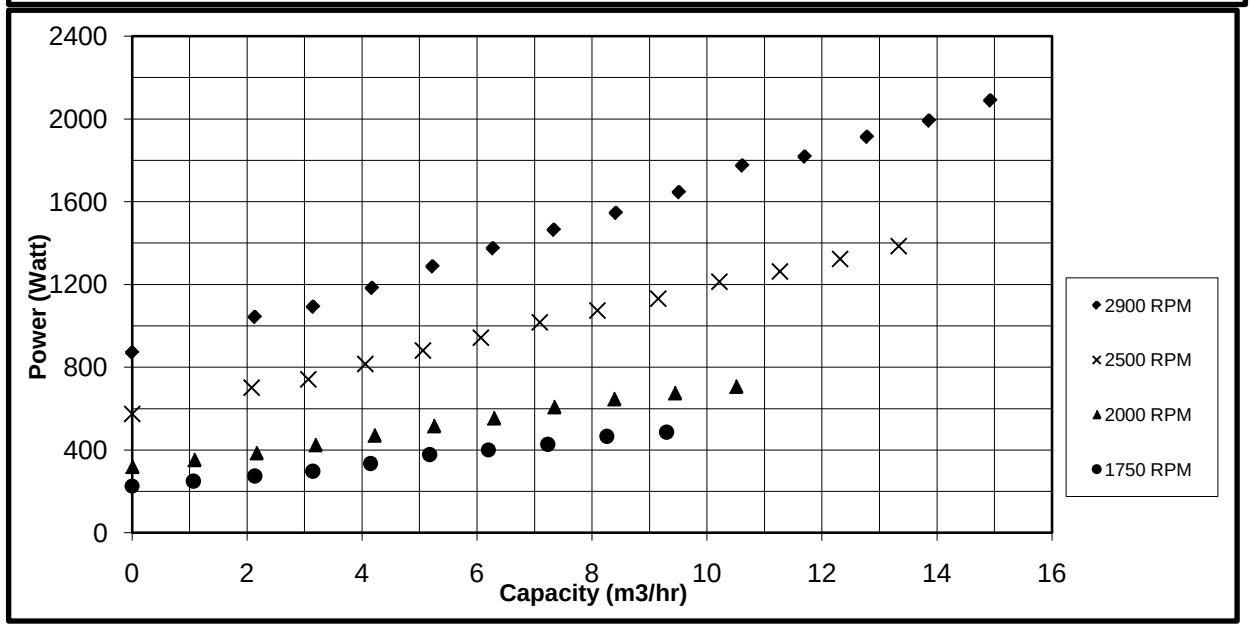

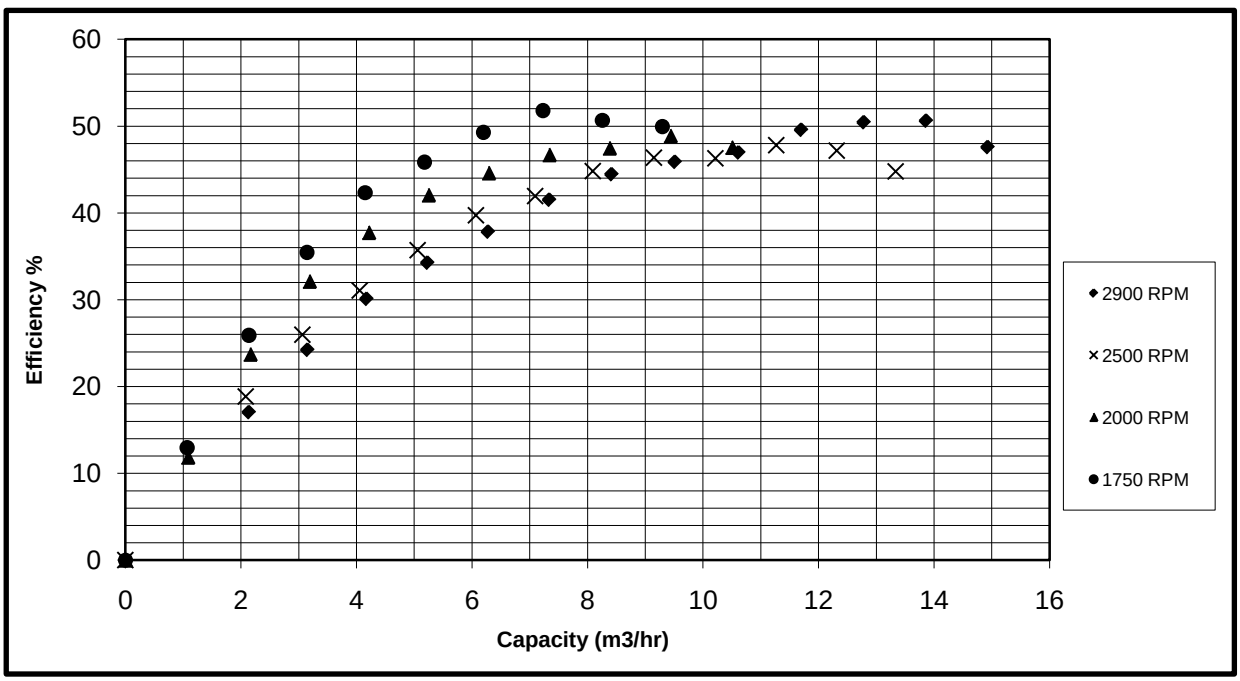

Figure (5-10) Experimental Pump performance for impeller configuration B at different RPM

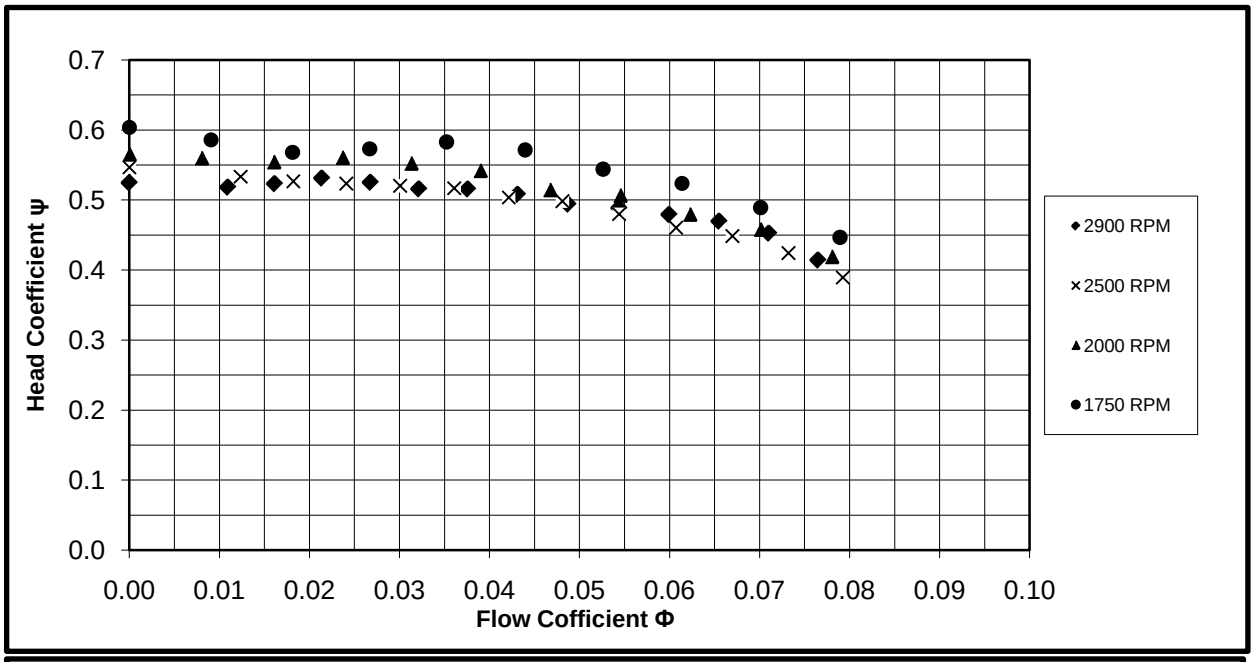

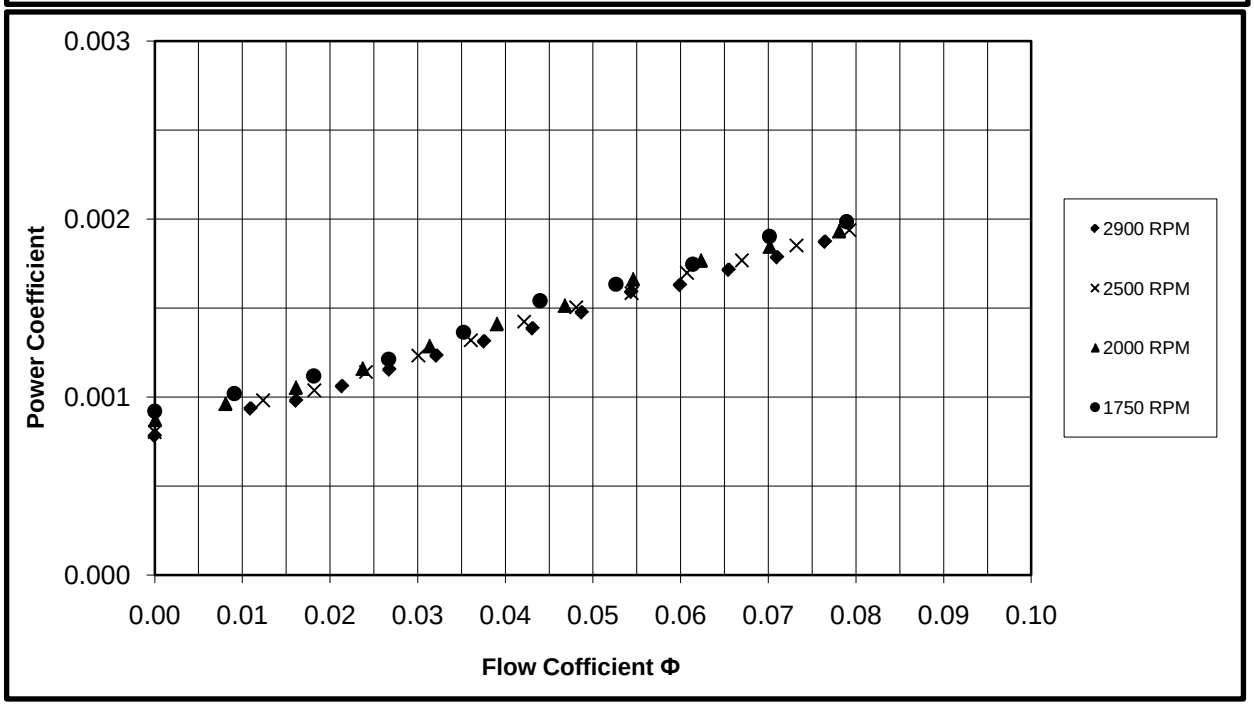

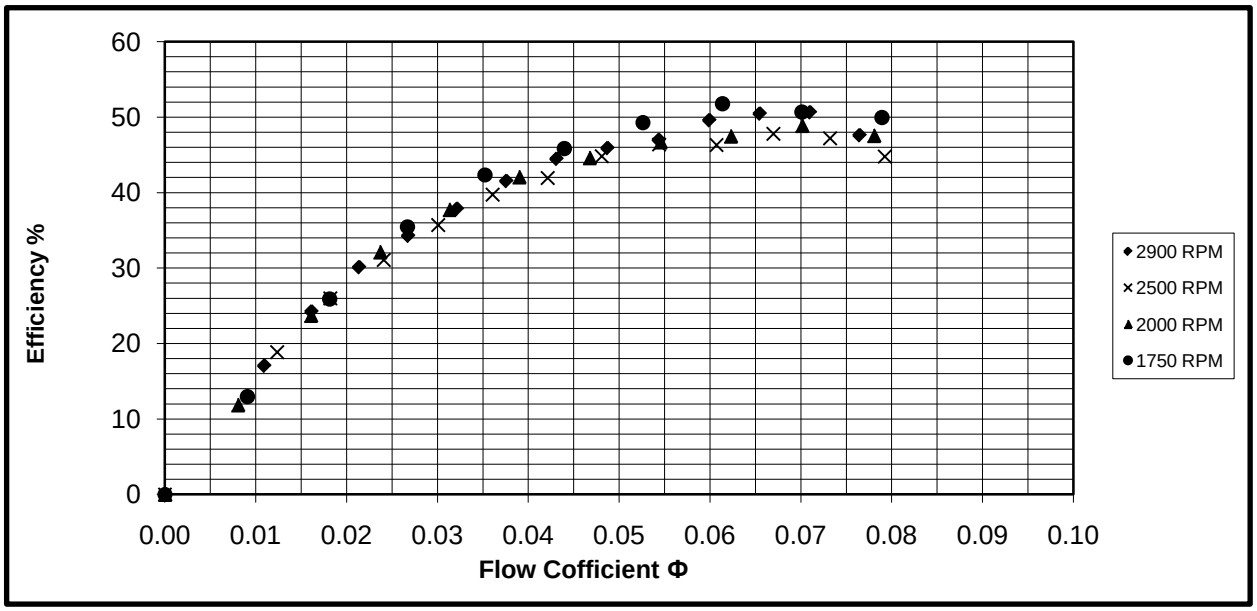

Figure (5-11) Experimental Dimensionless coefficients for impeller configuration B at different RPM

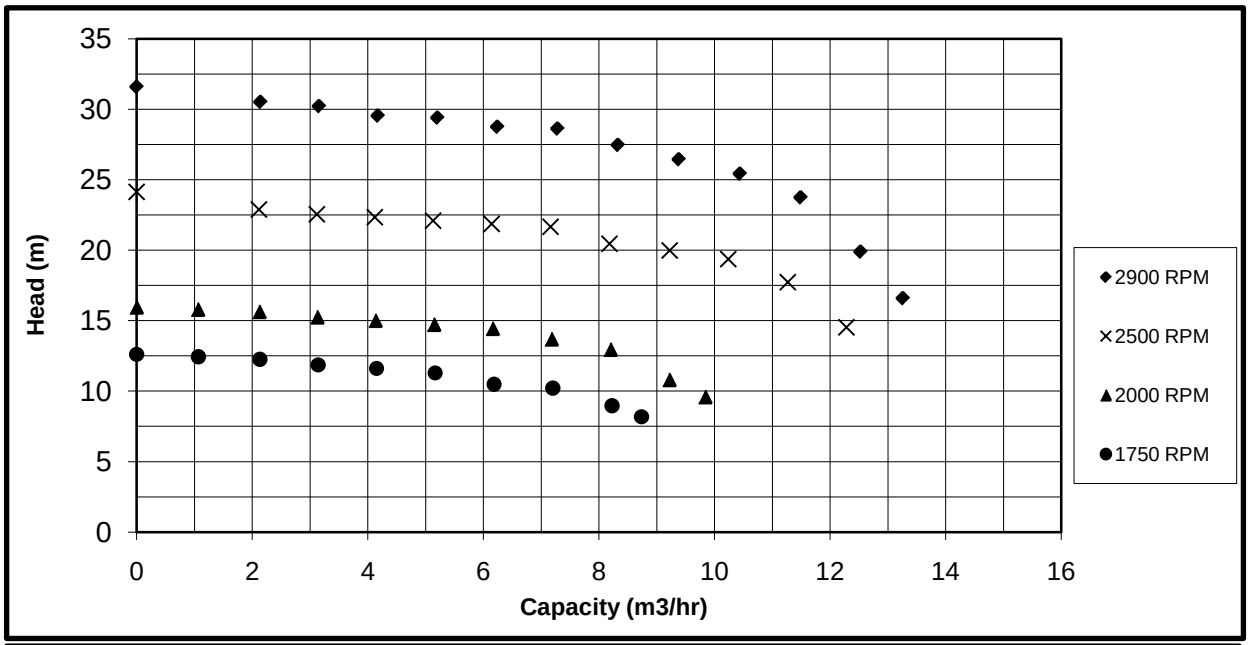

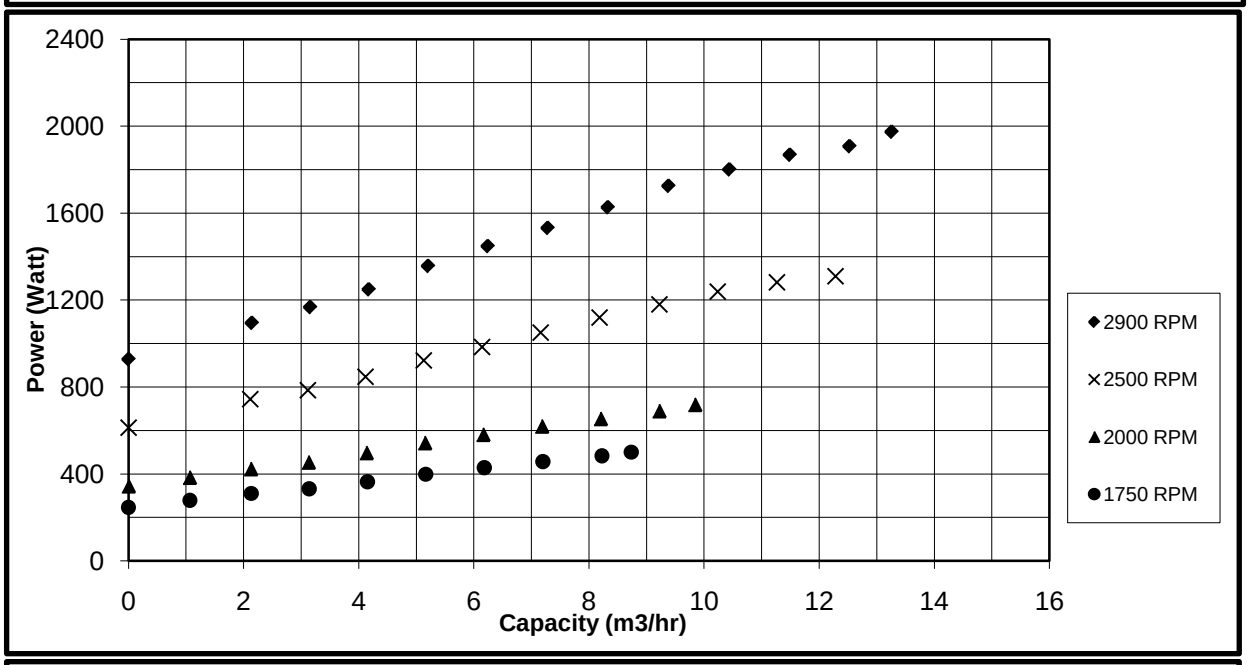

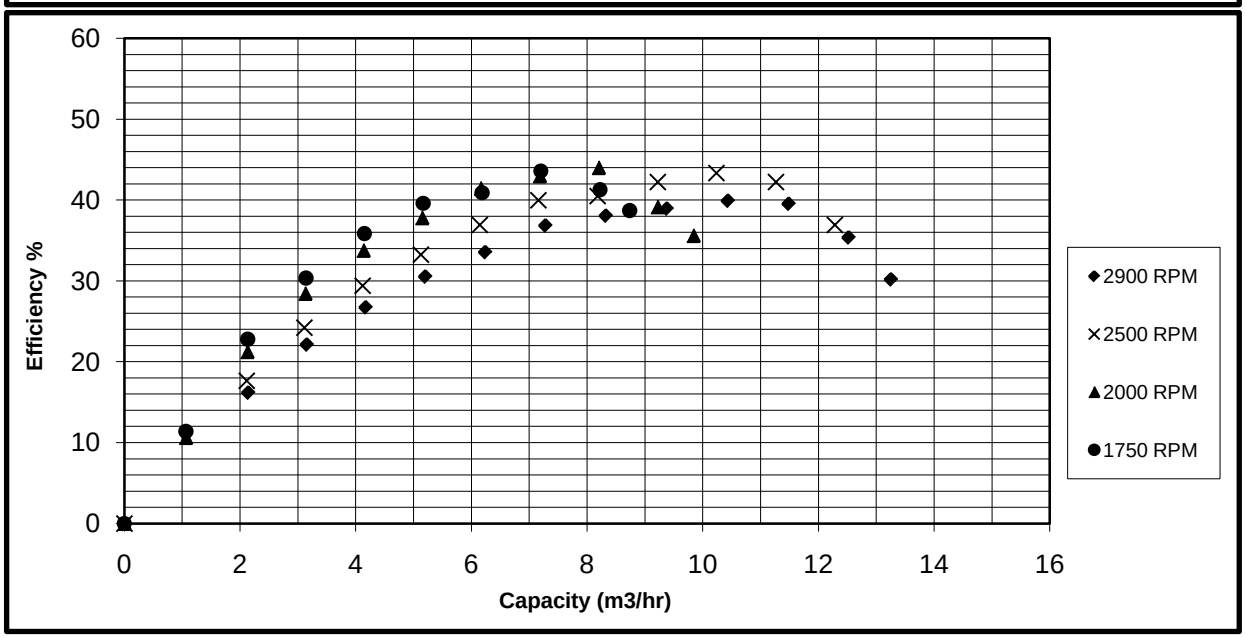

Figure (5-12) Experimental Pump performance for impeller configuration C at different RPM

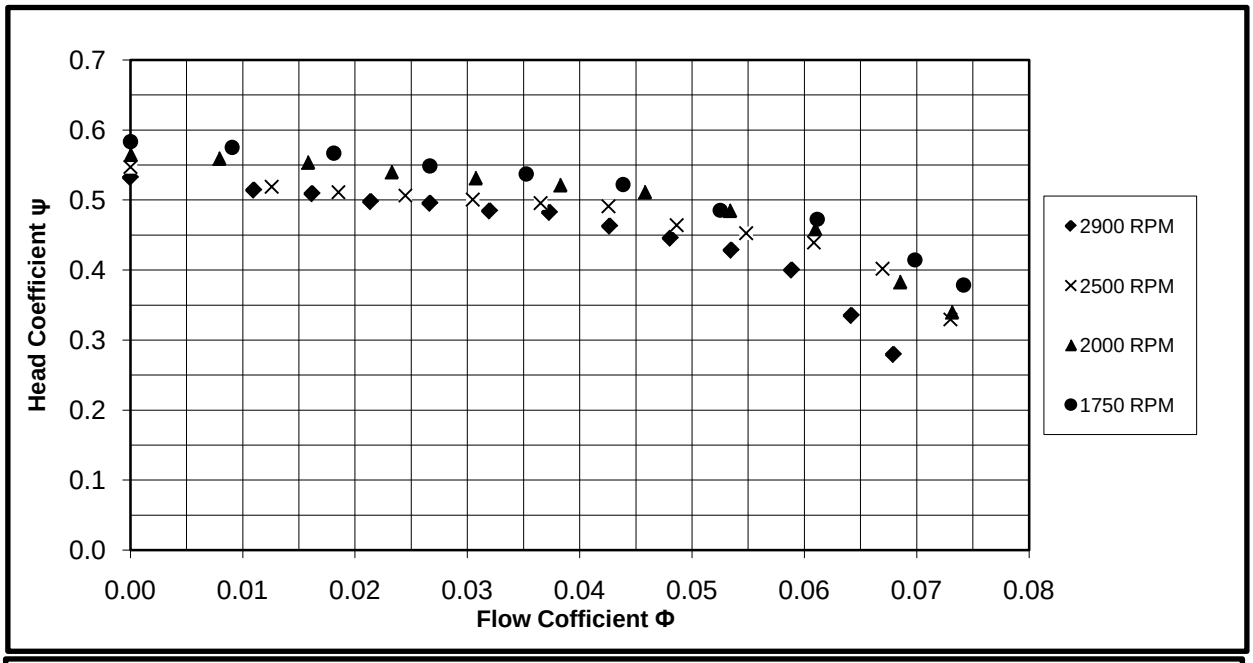

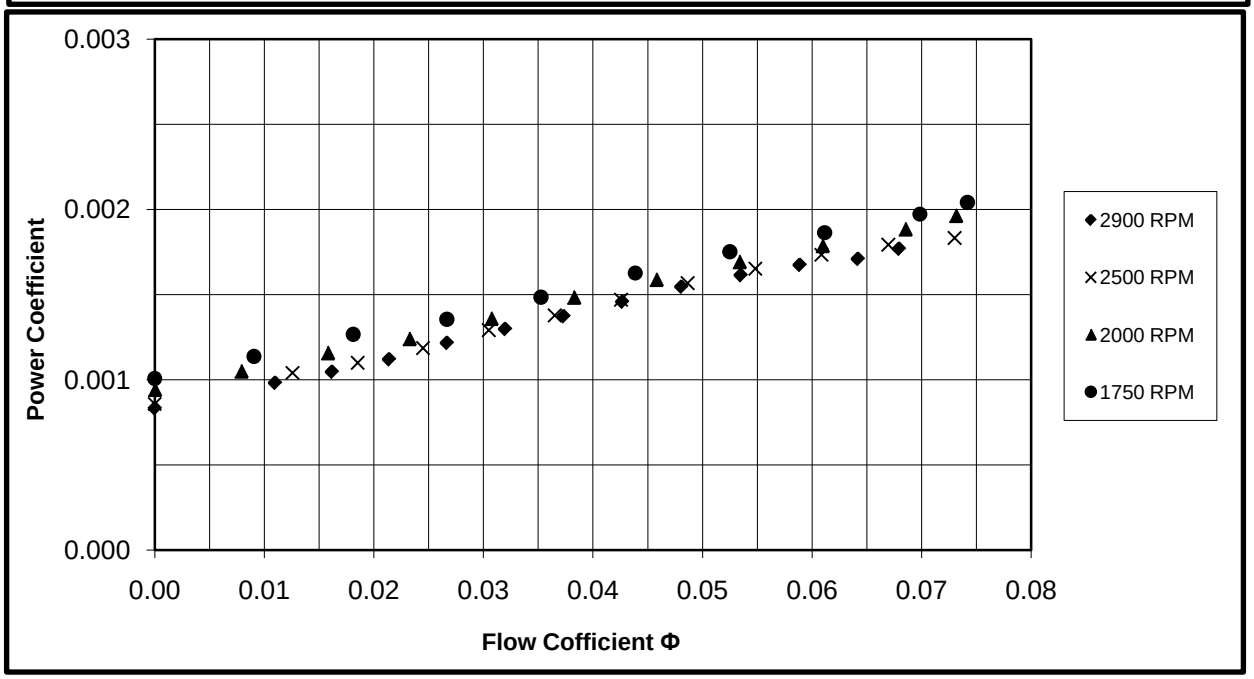

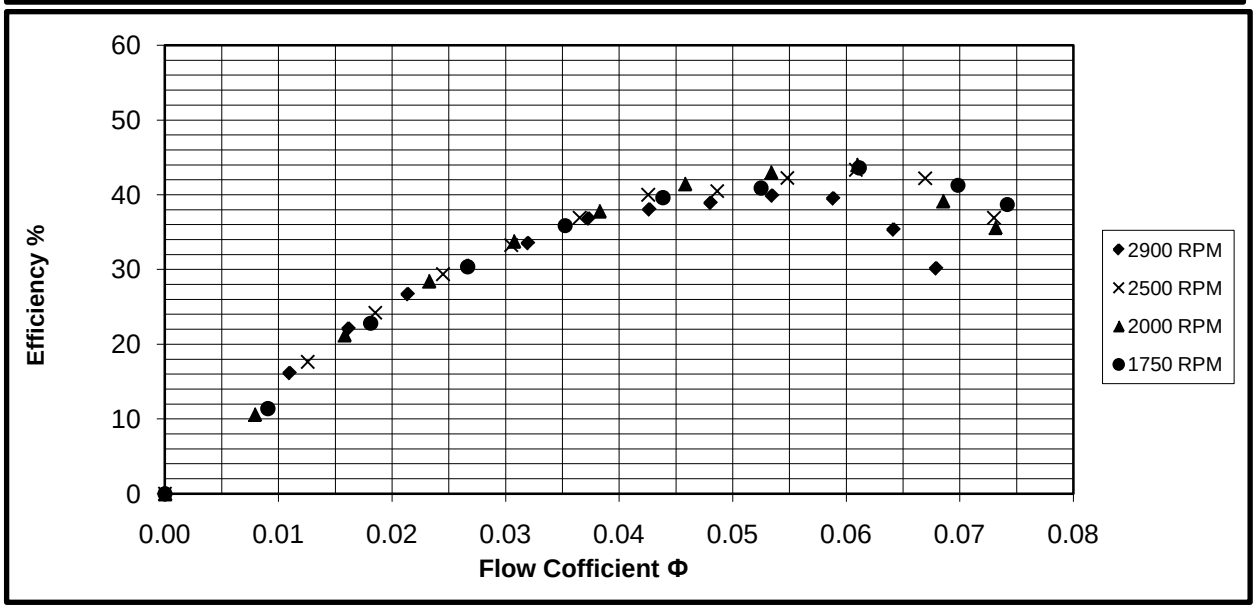

Figure (5-13) Experimental Dimensionless coefficients for impeller configuration C at different RPM

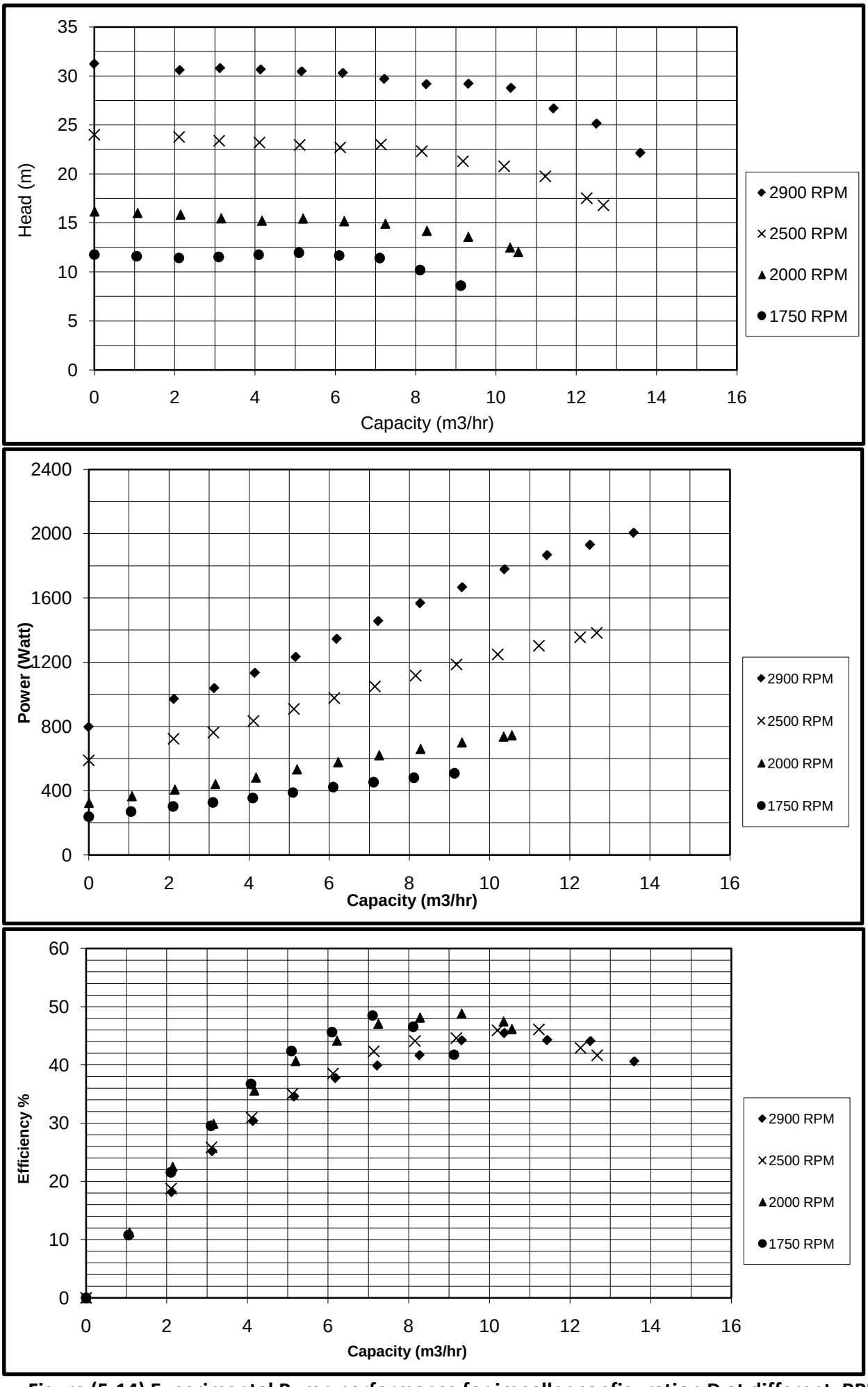

Figure (5-14) Experimental Pump performance for impeller configuration D at different RPM

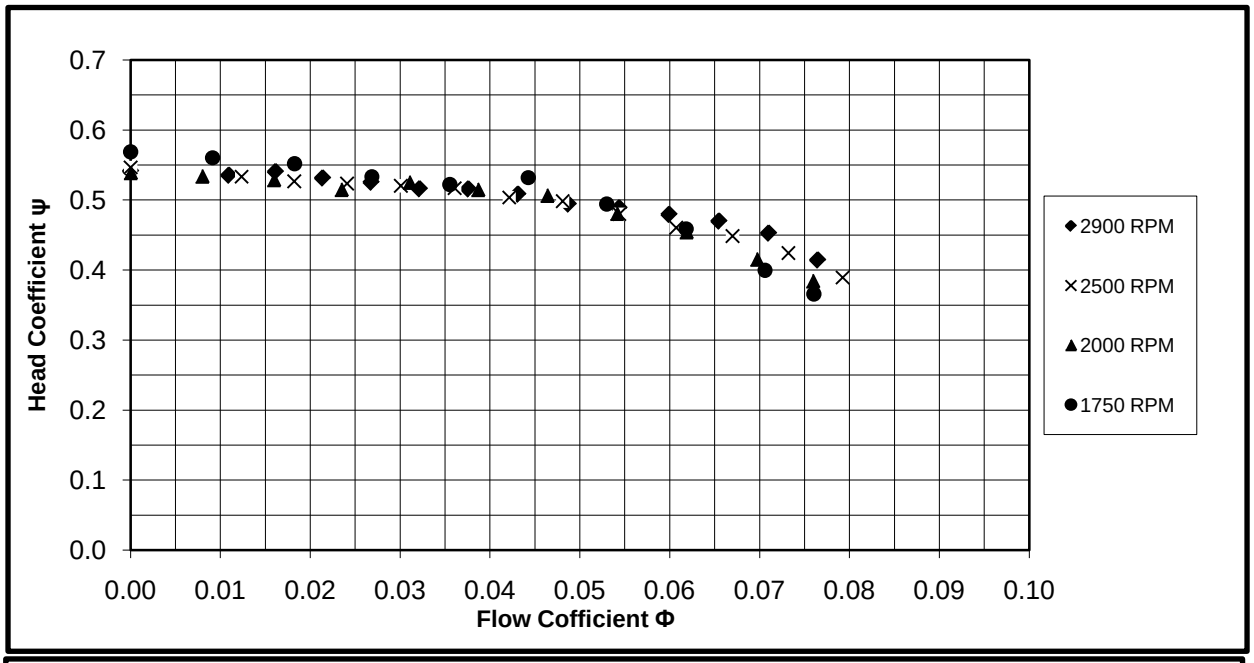

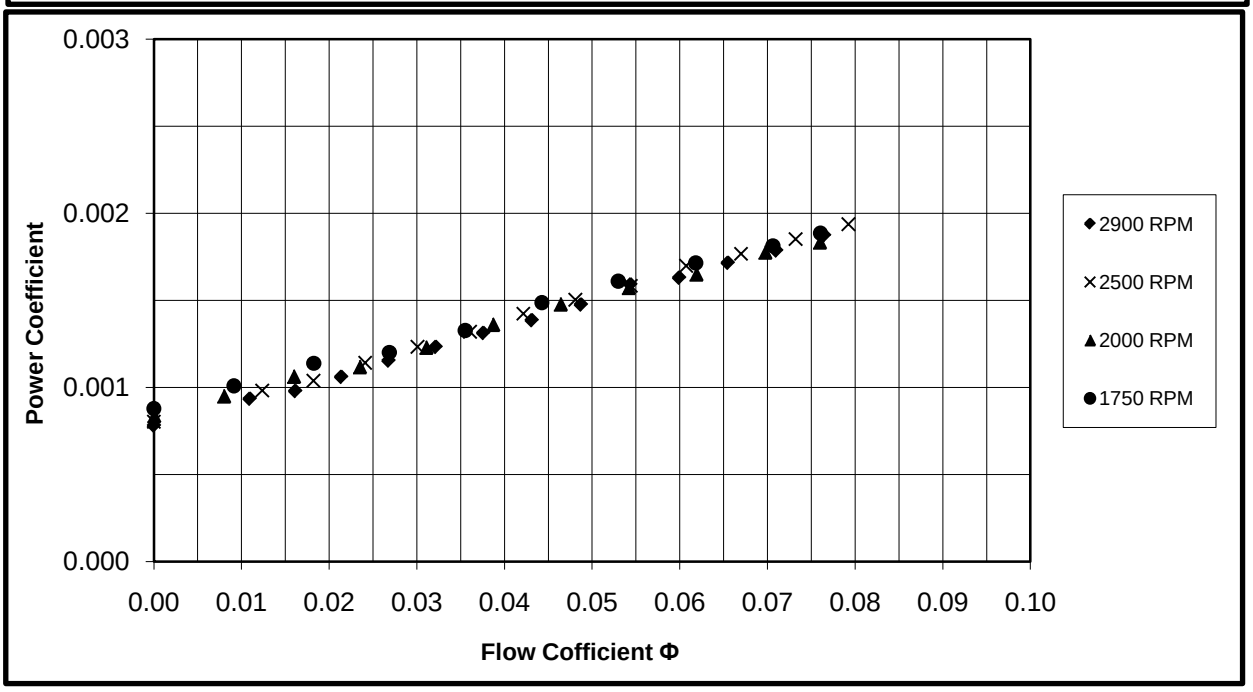

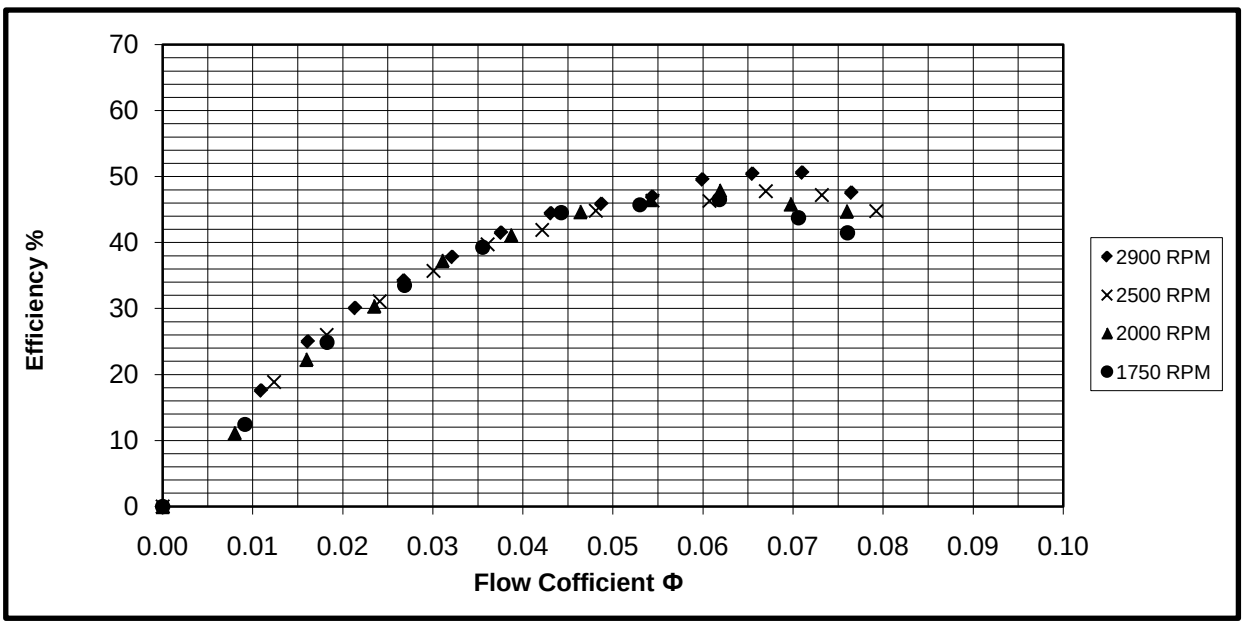

Figure (5-15) Experimental Dimensionless coefficients for impeller configuration D at different RPM

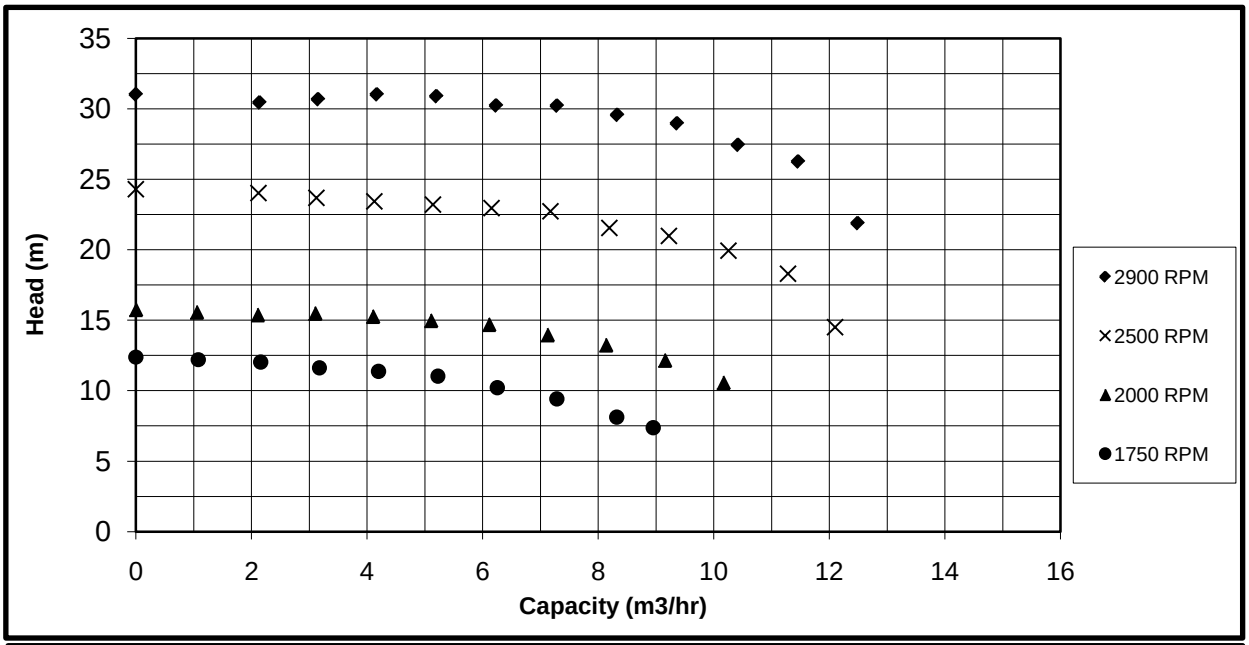

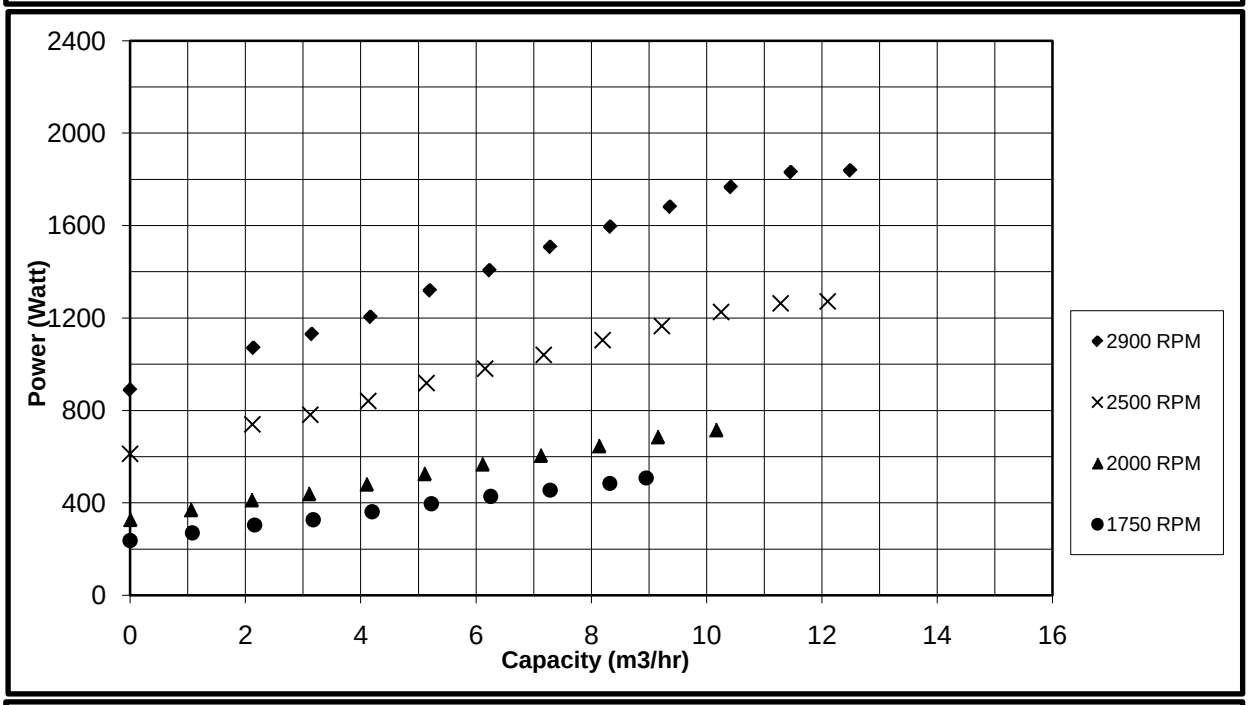

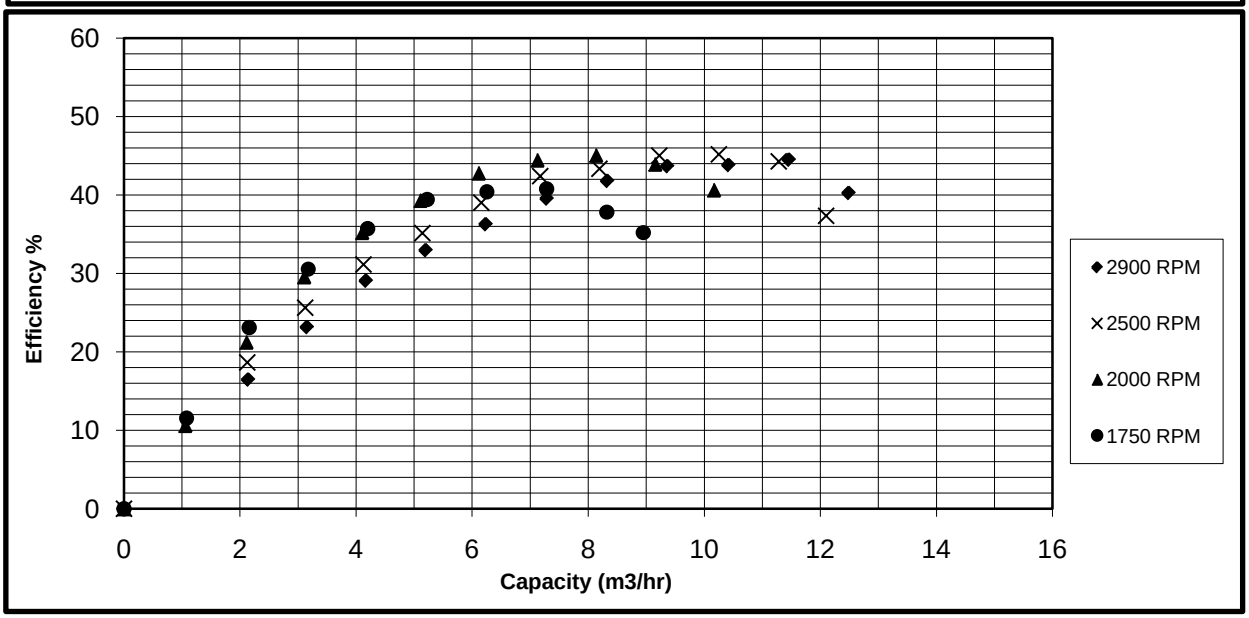

Figure (5-16) Experimental Pump performance for impeller configuration E at different RPM

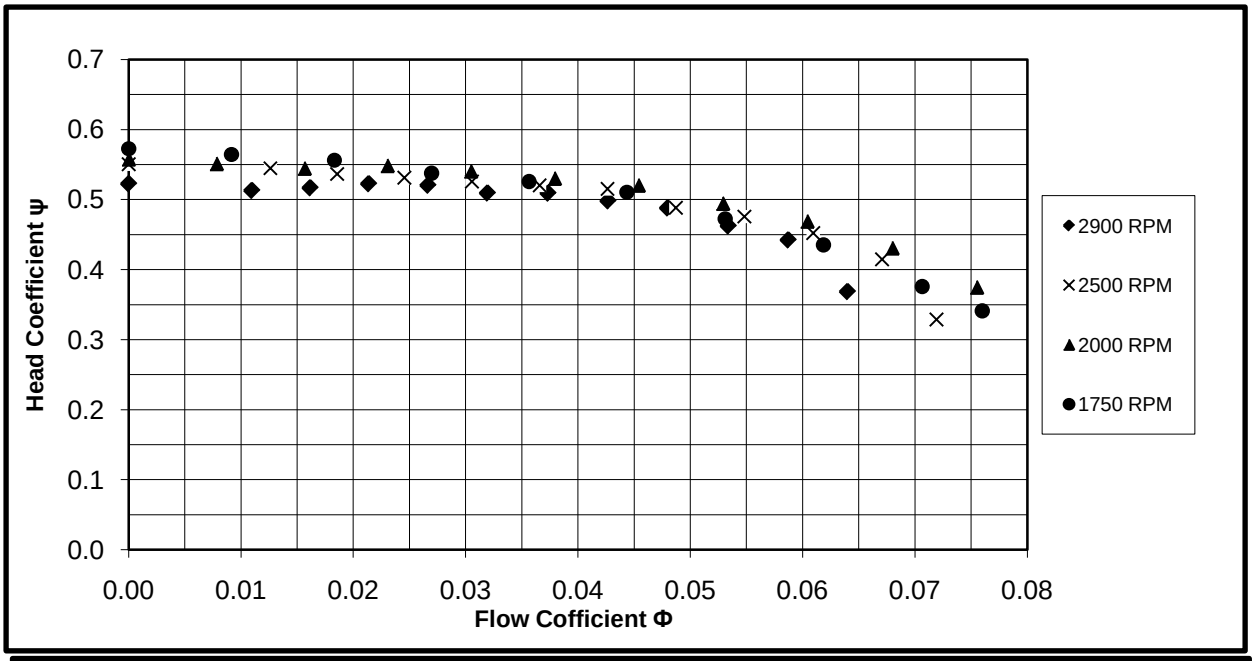

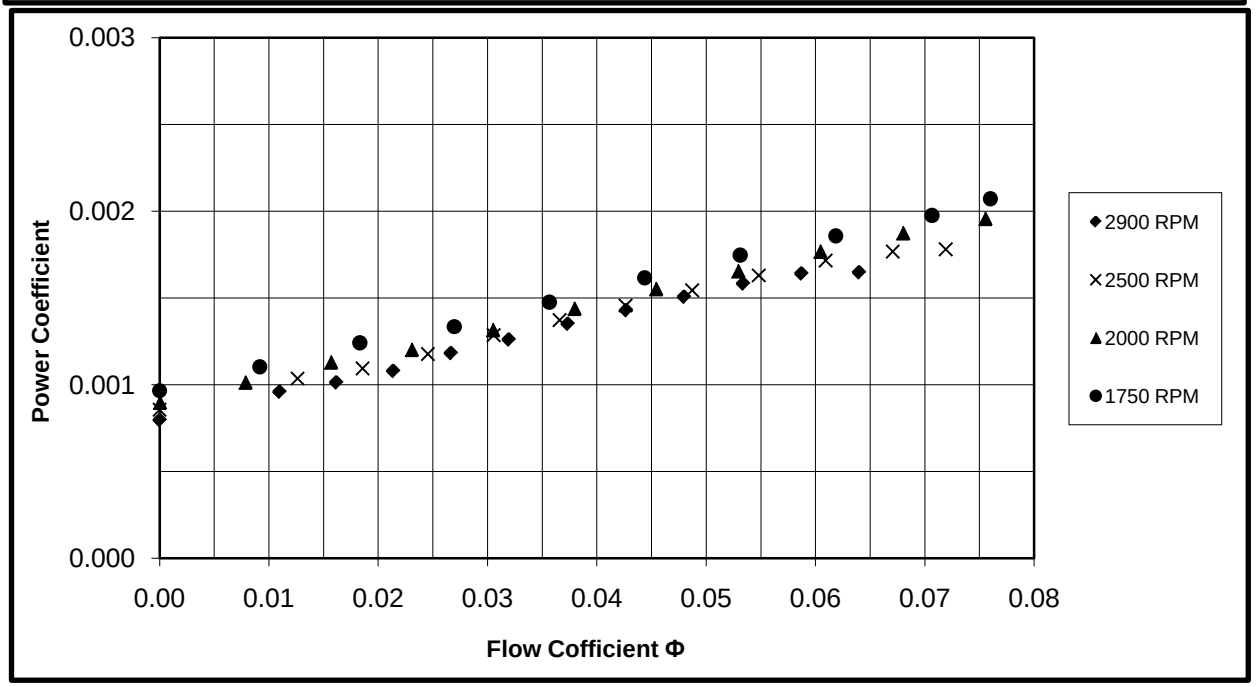

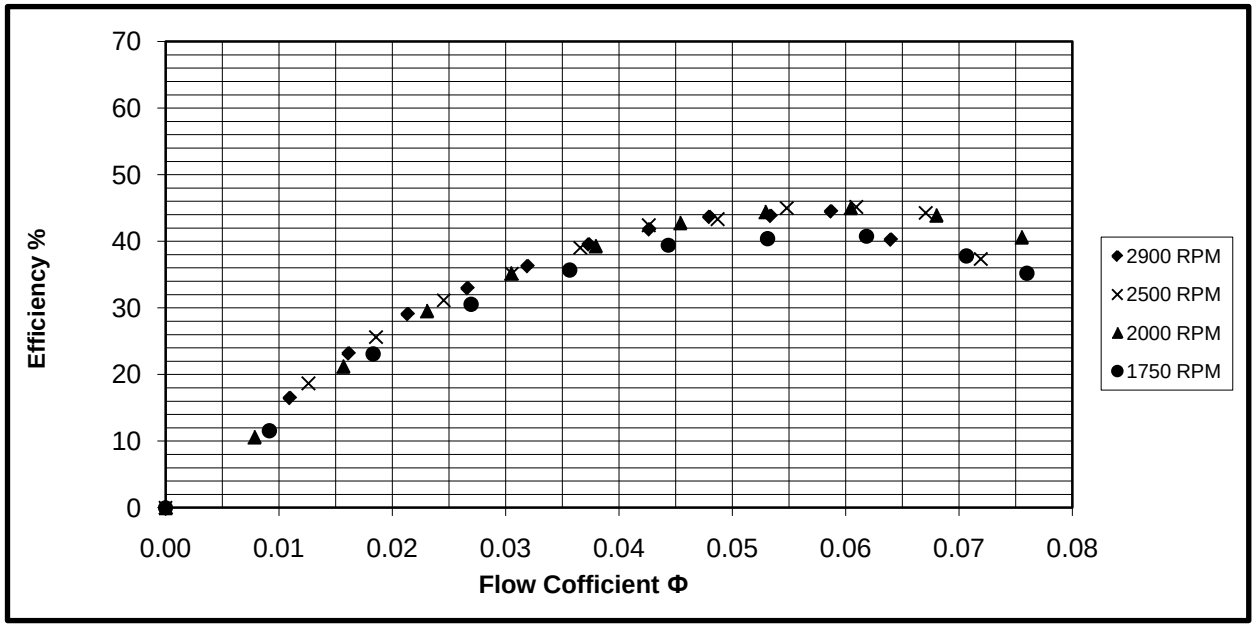

Figure (5-17) Experimental Dimensional less coefficients for impeller configuration E at different RPM

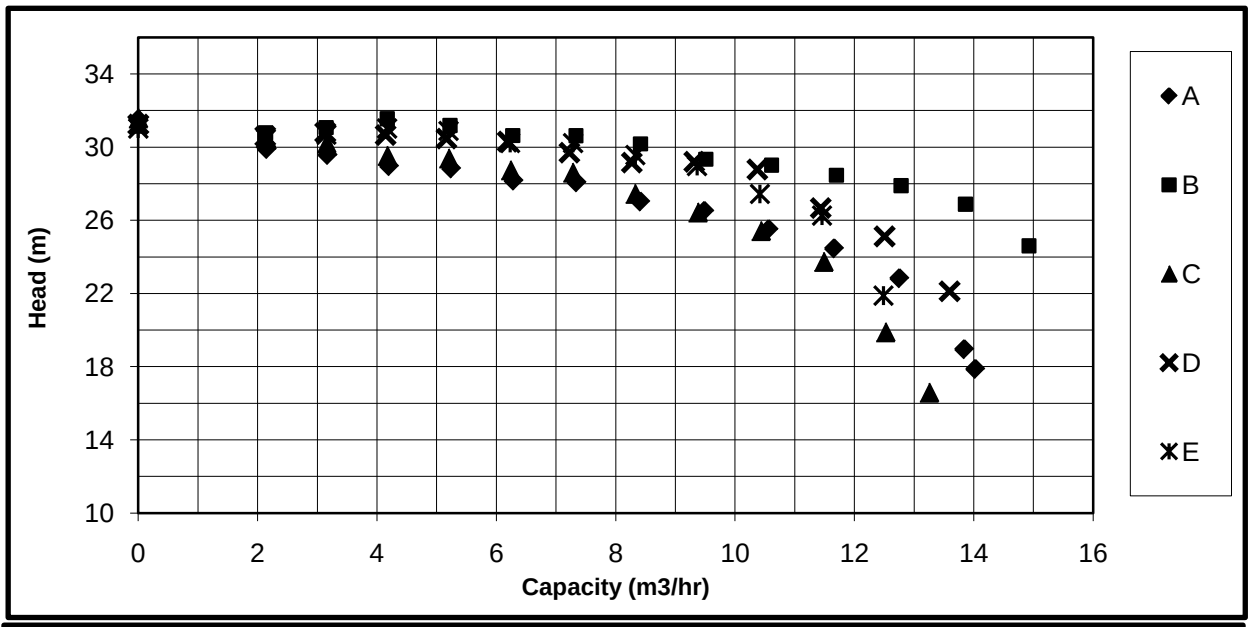

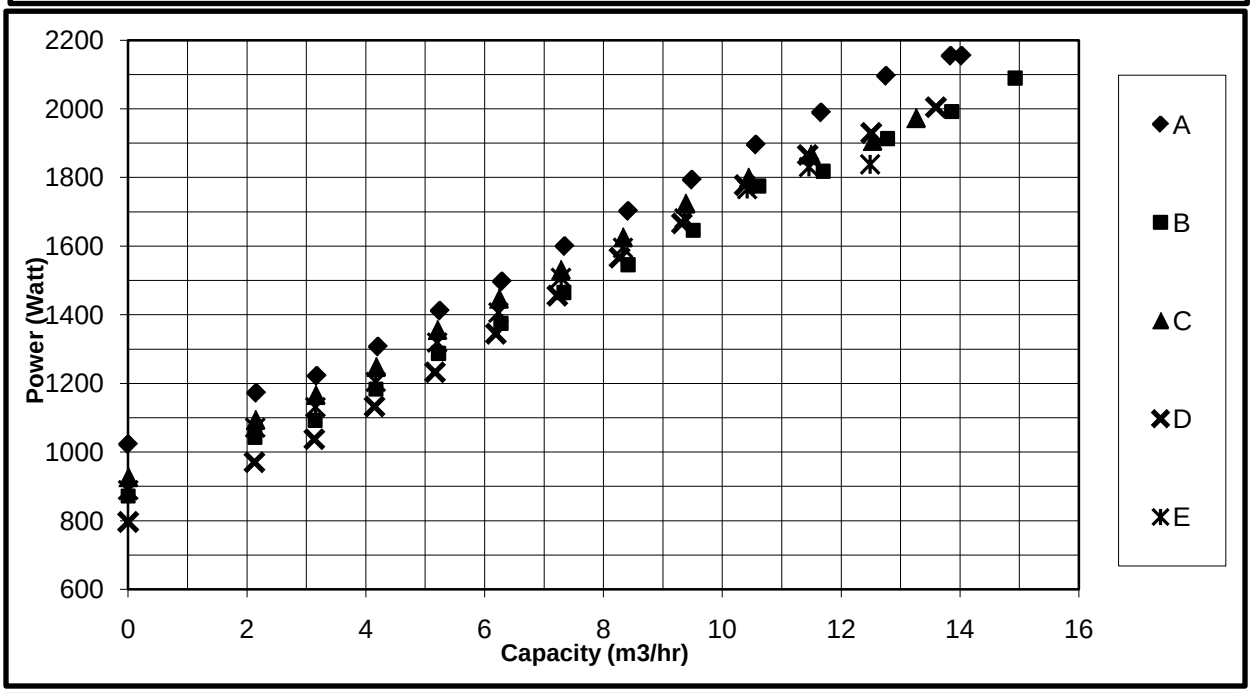

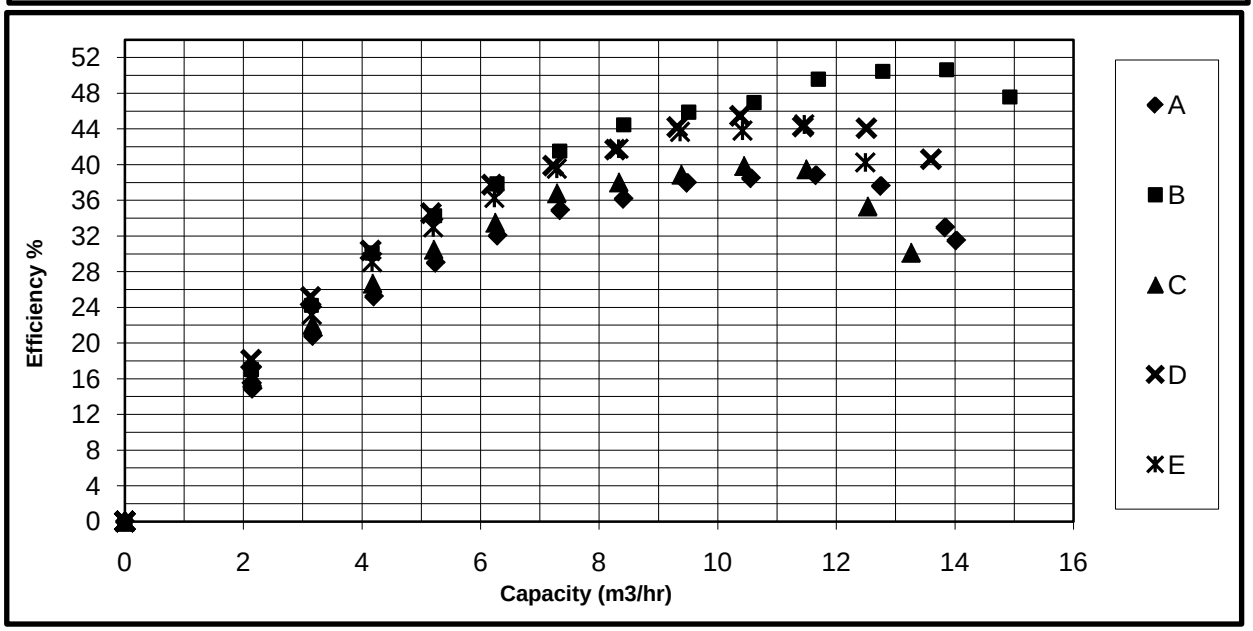

Figuer (5-18) Comparison for experimental results for all impeller configurations at 2900 RPM

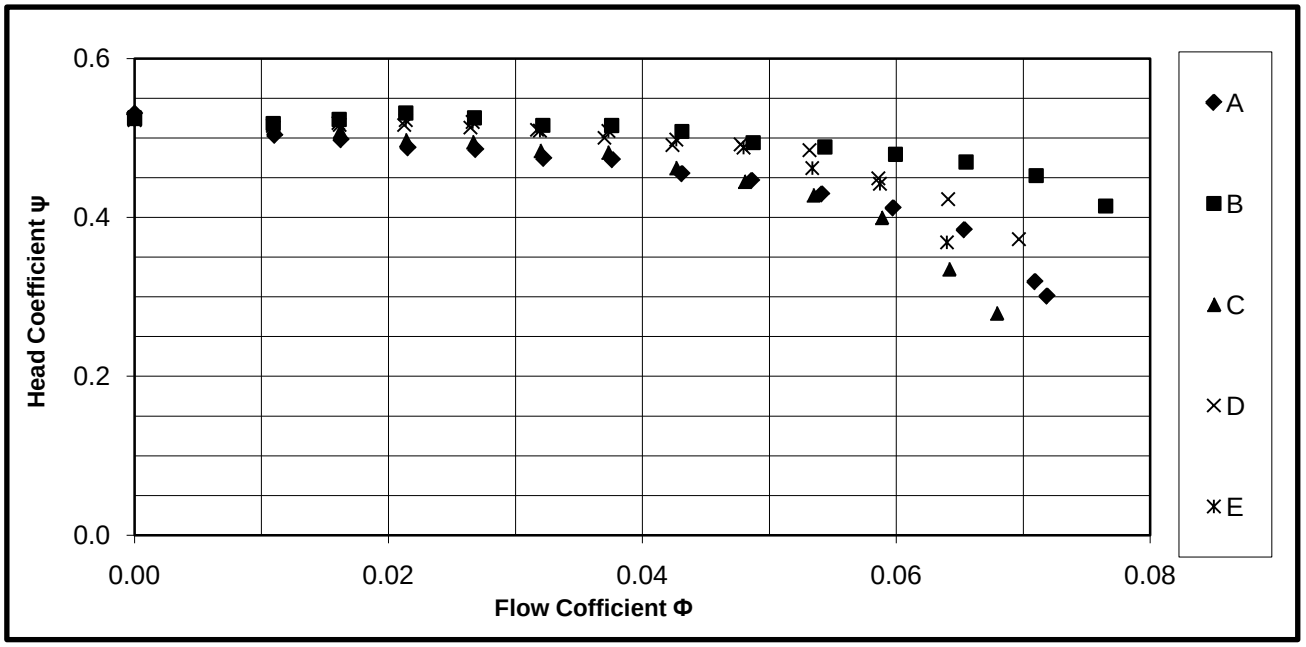

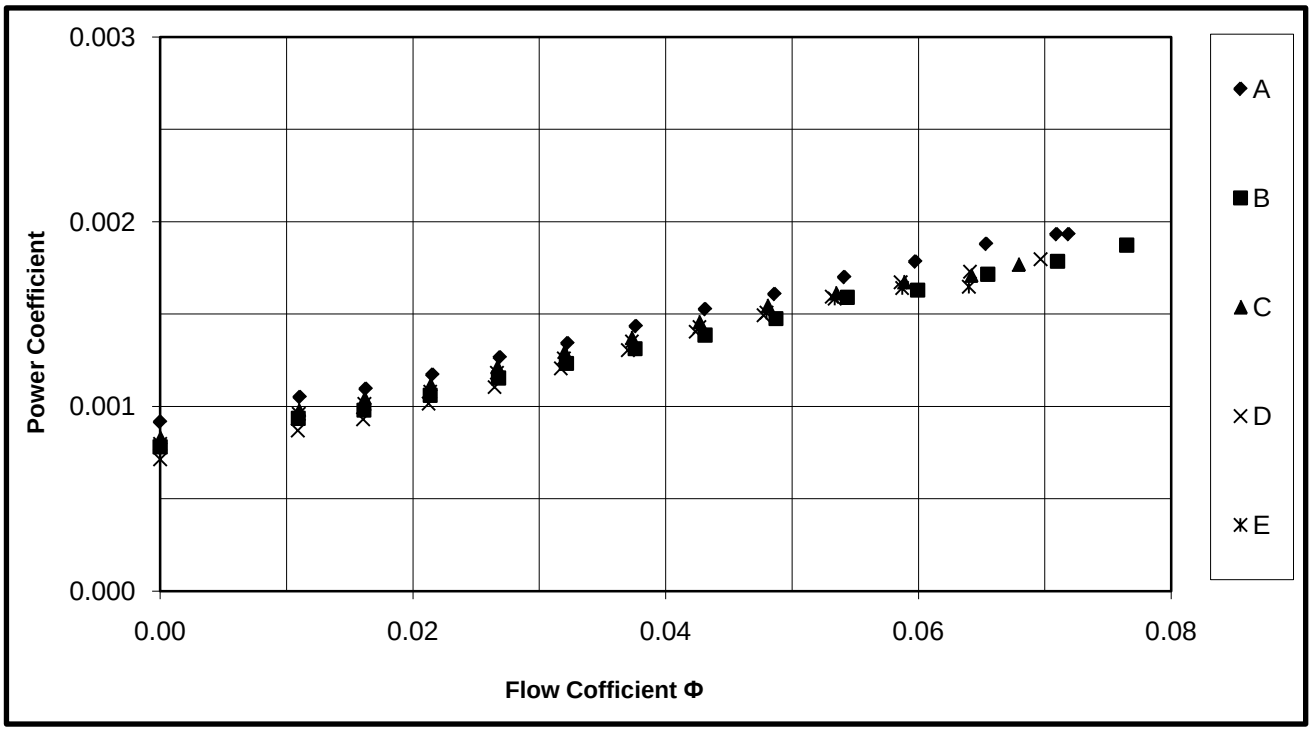

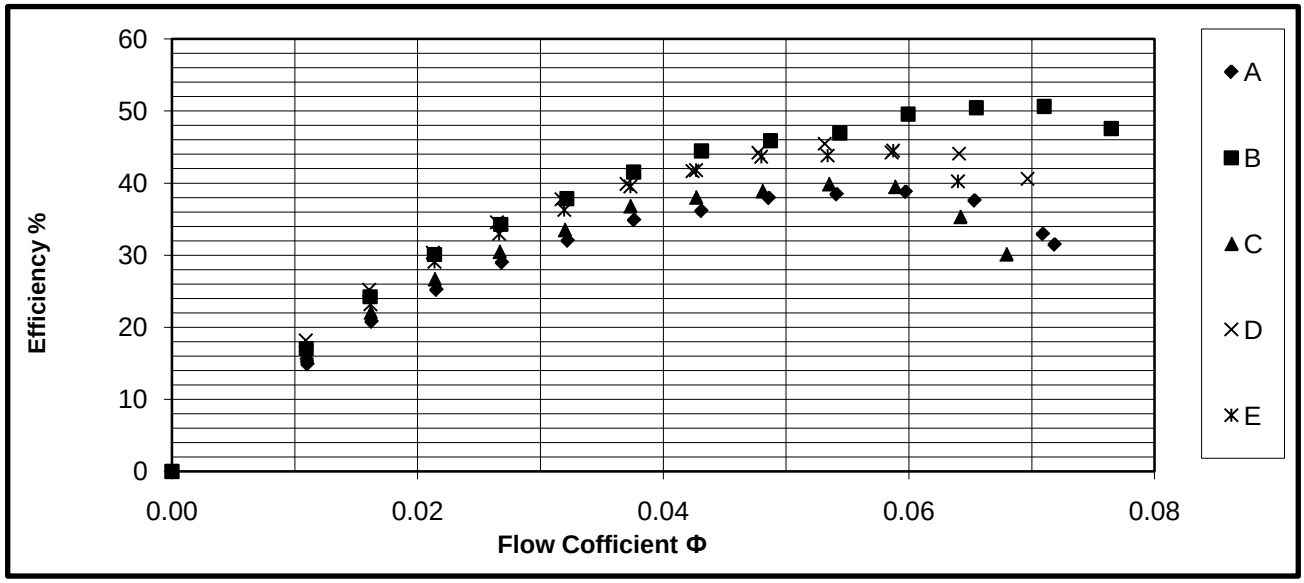

Figure (5-19) Experimental Dimensionless coefficients all impeller configurations at 2900 RPM

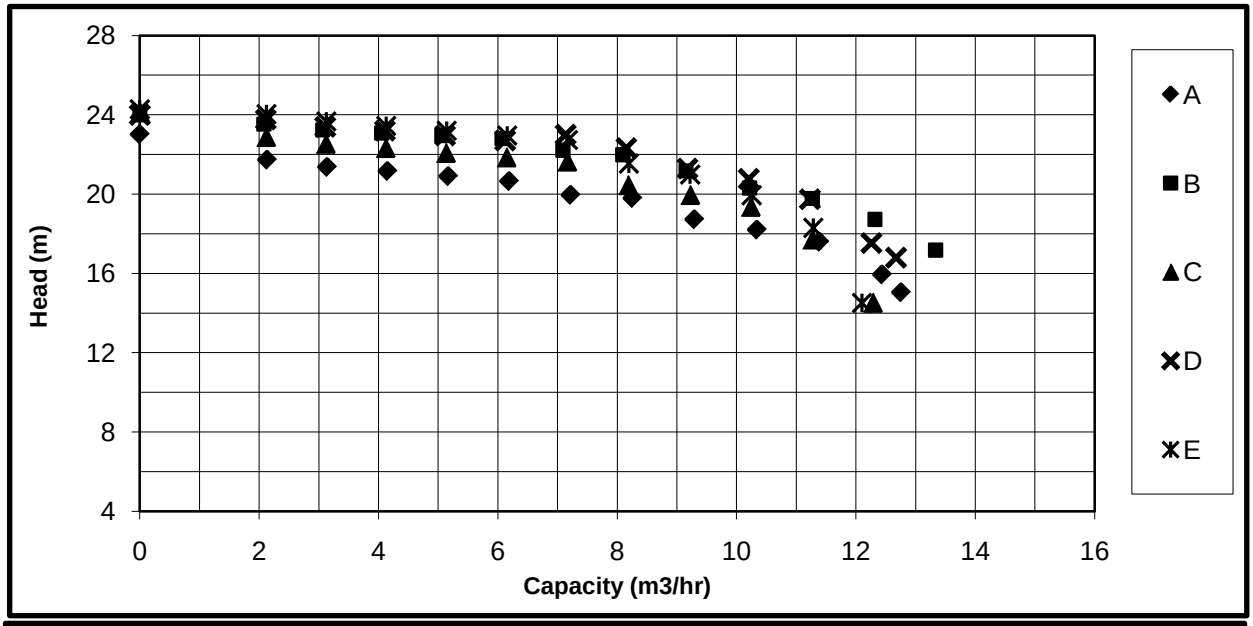

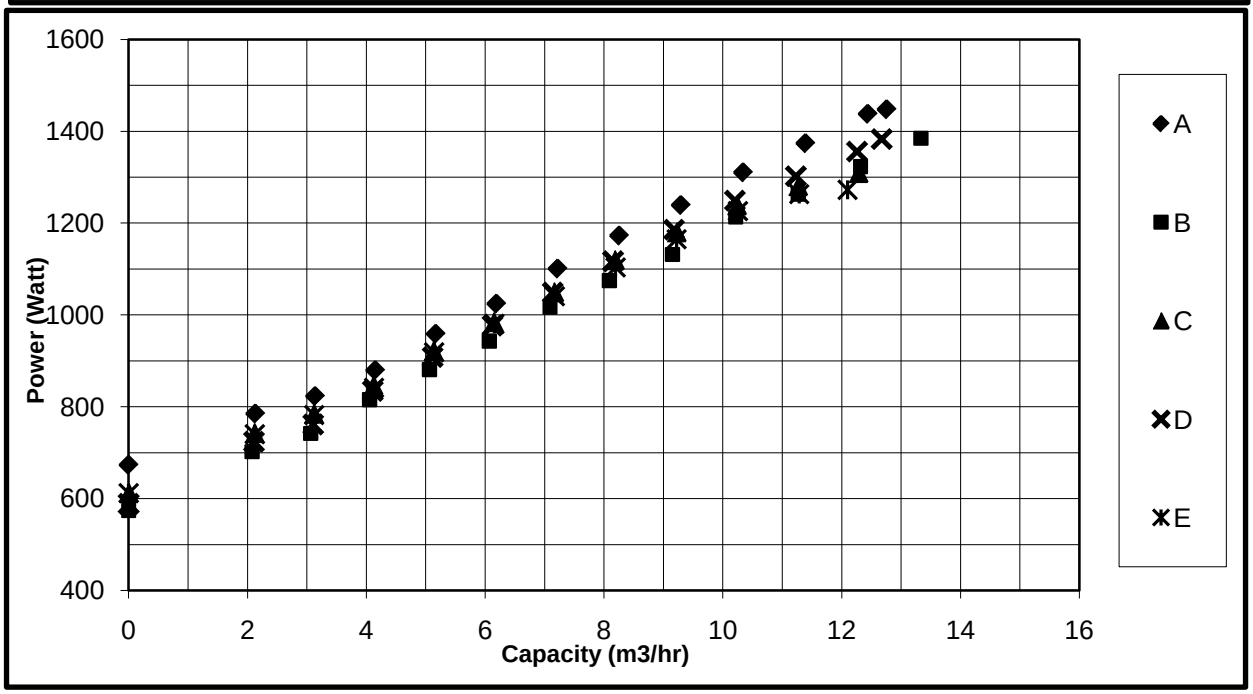

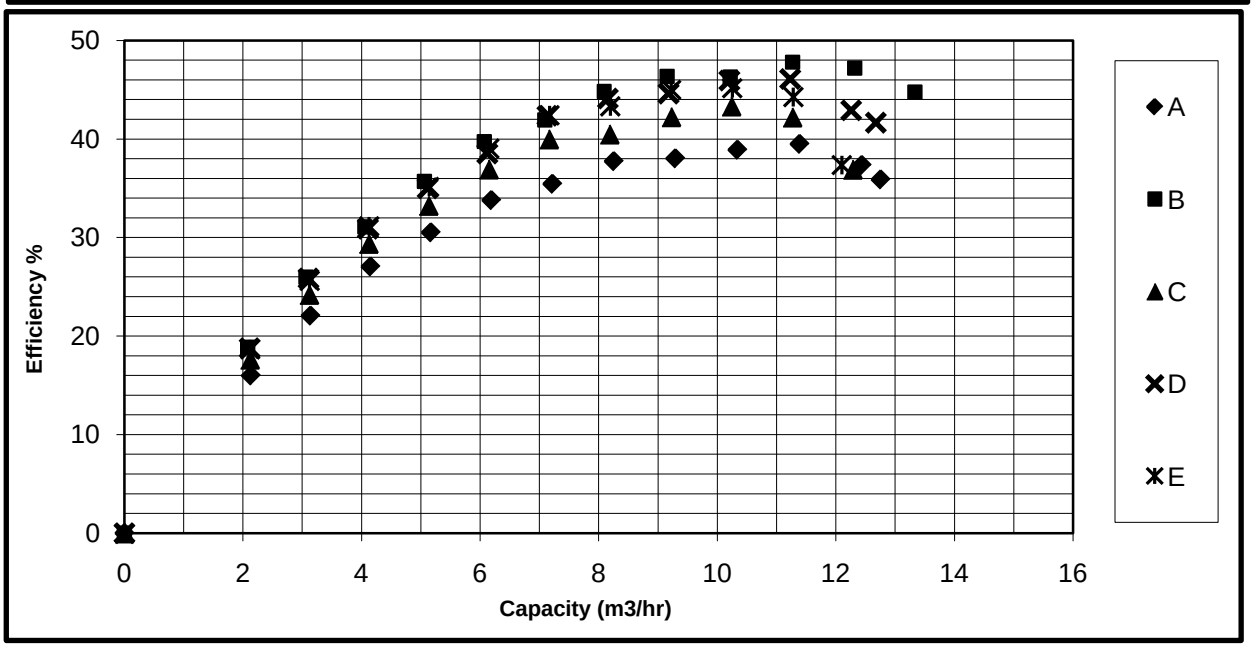

Figure (5-20) Comparison for experimental results for all impeller configurations at 2500 RPM

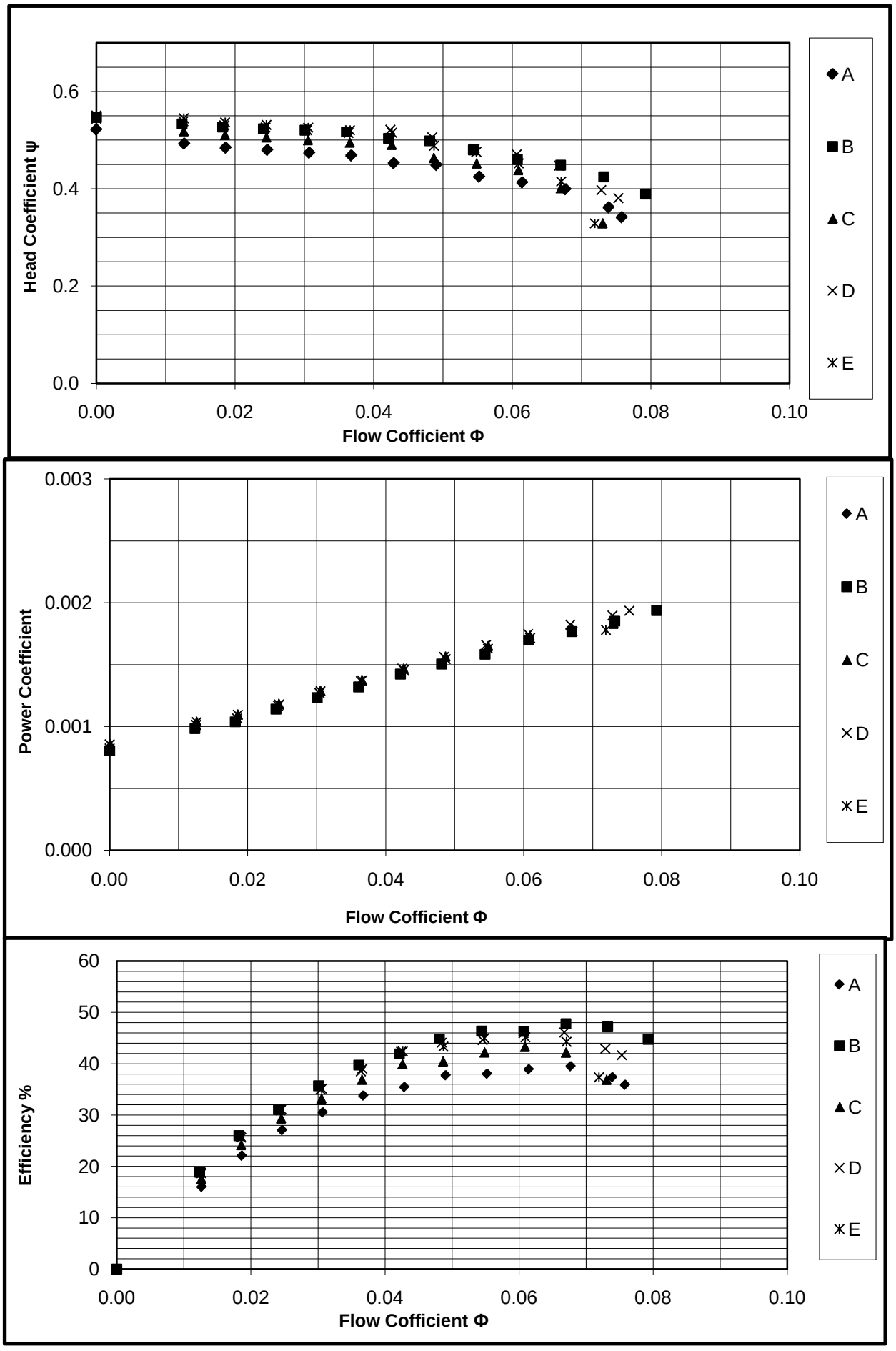

Figure (5-21) Experimental Dimensionless coefficients all impeller configurations at 2500 RPM

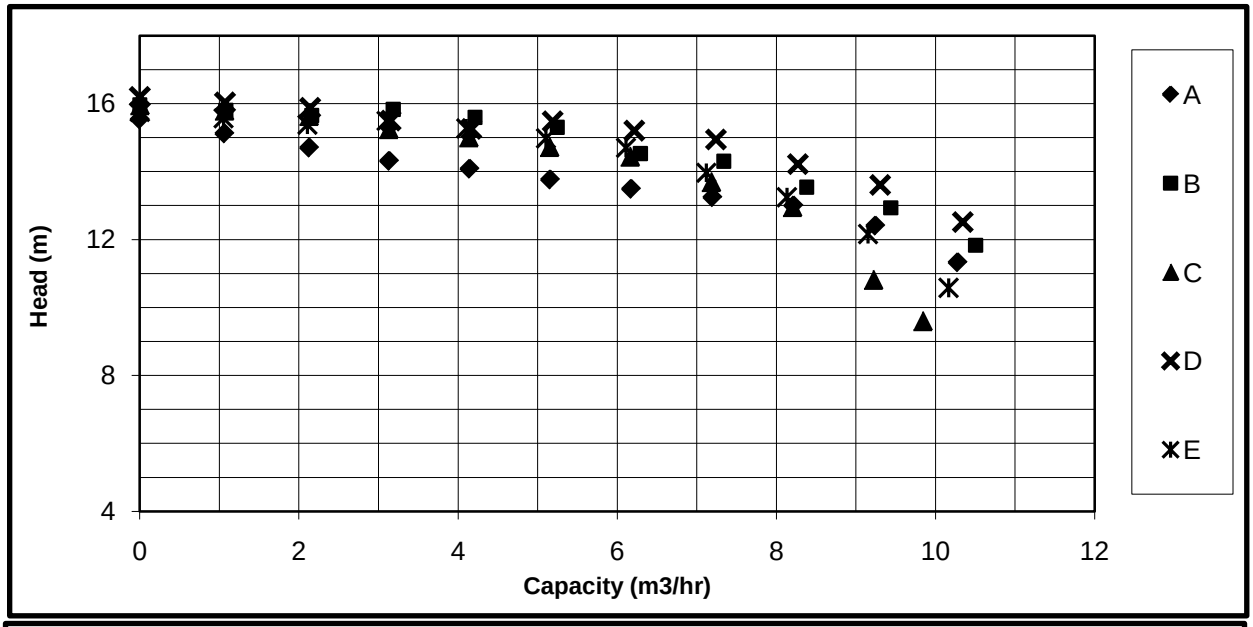

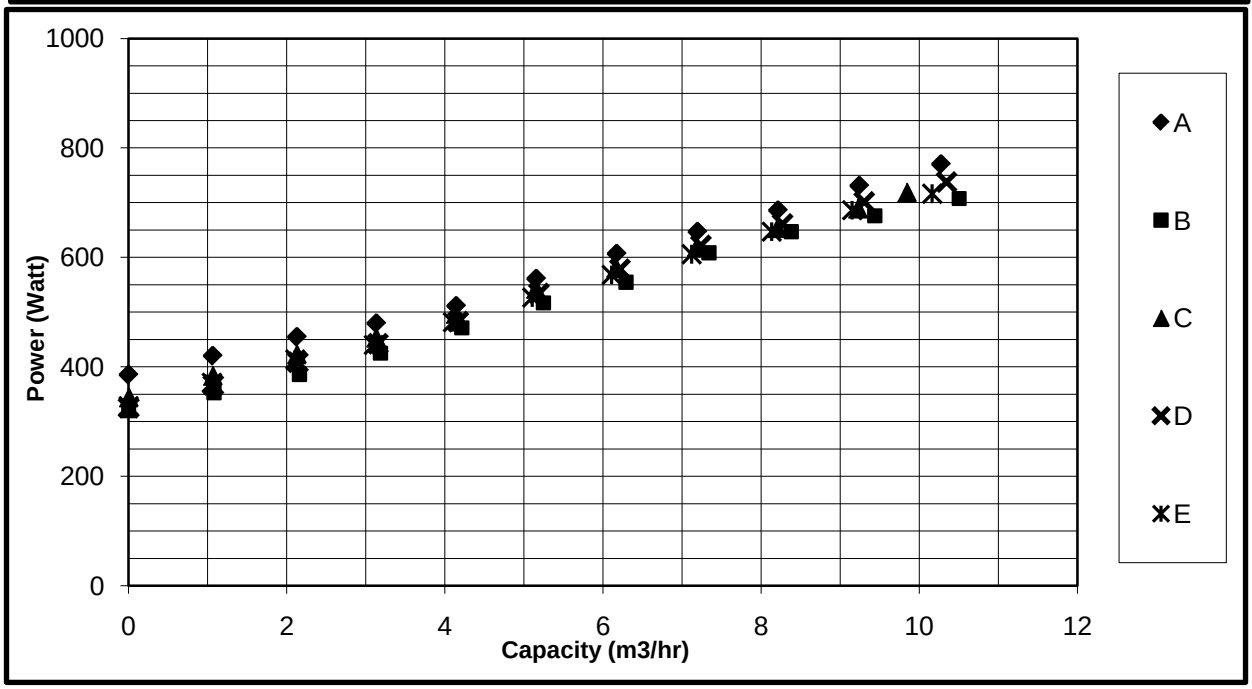

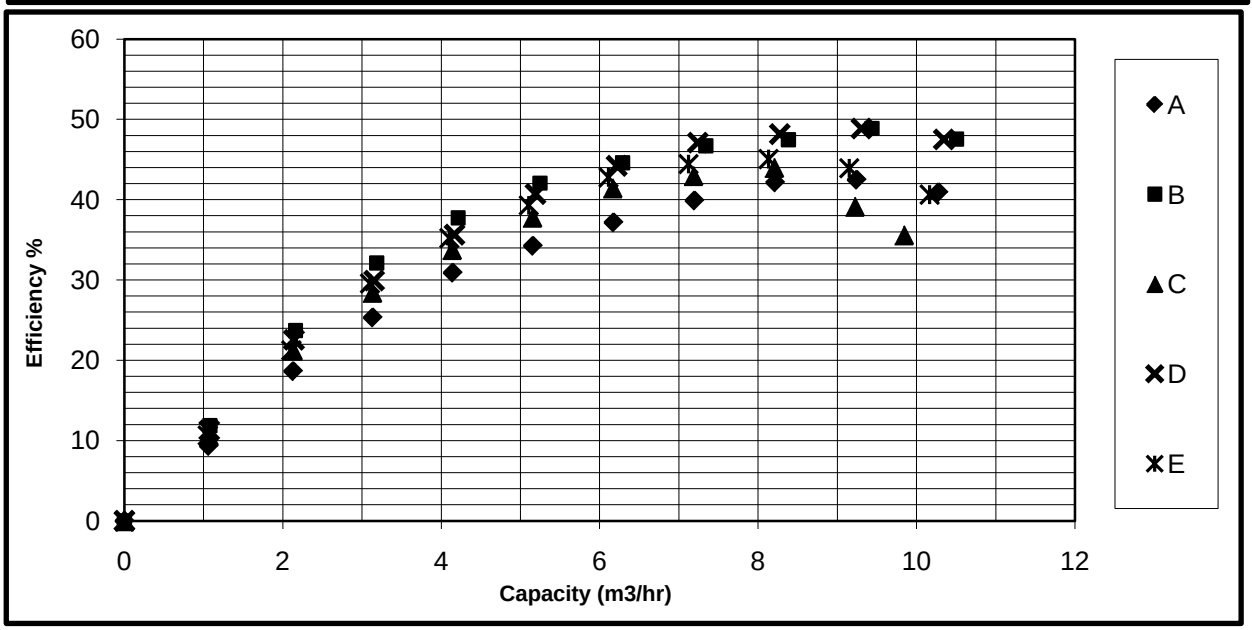

Figure (5-22) Comparison for experimental results for all impeller configurations at 2000 RPM

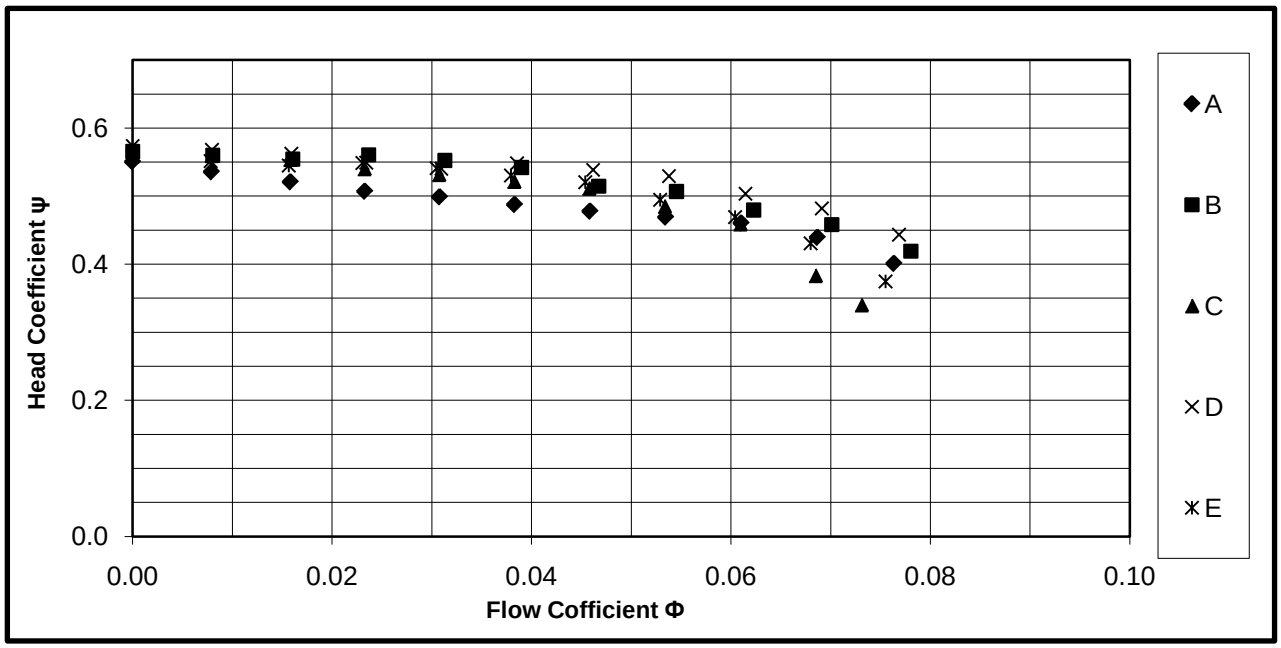

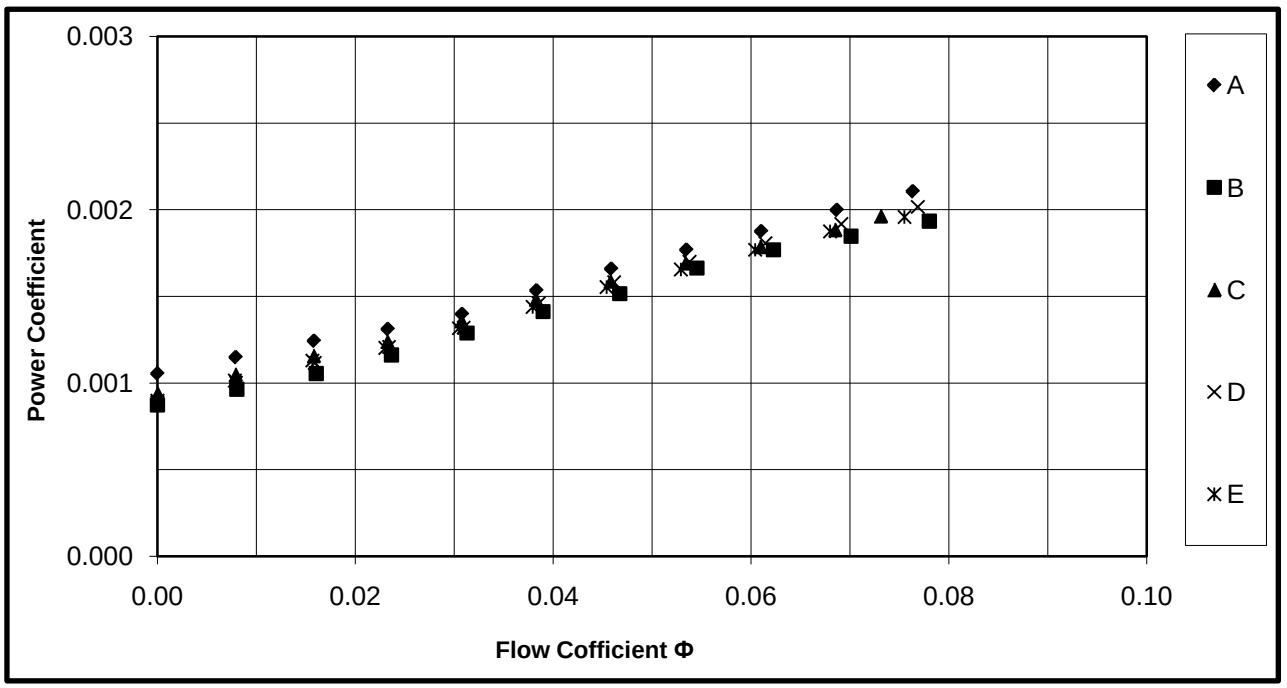

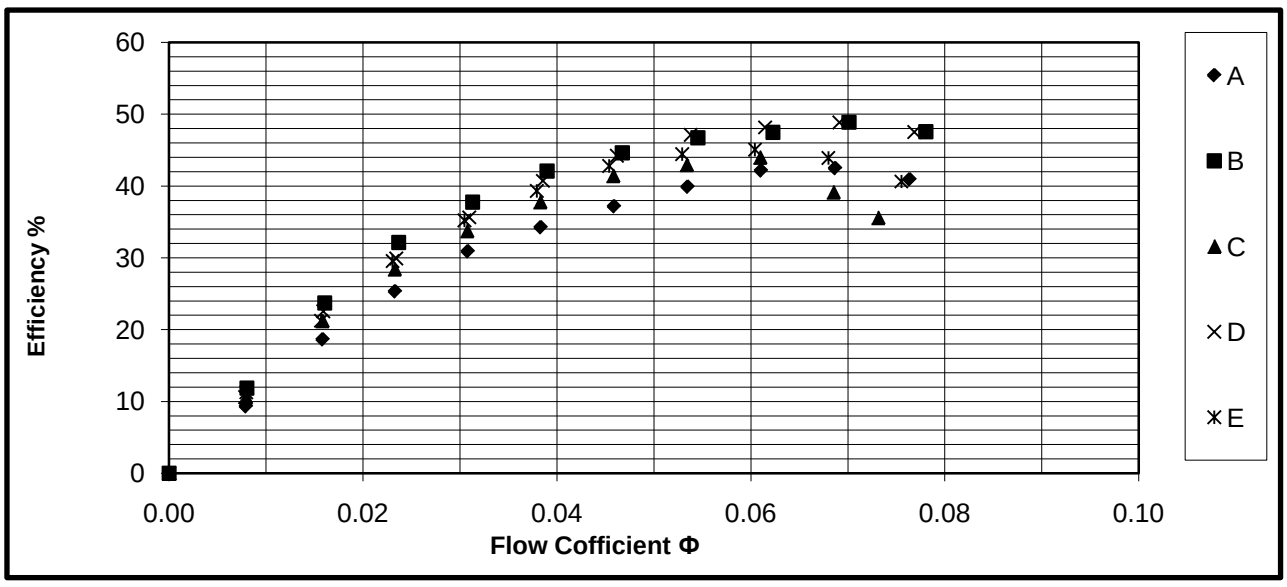

Figure (5-23) Experimental Dimensionless coefficients all impeller configurations at 2000 RPM

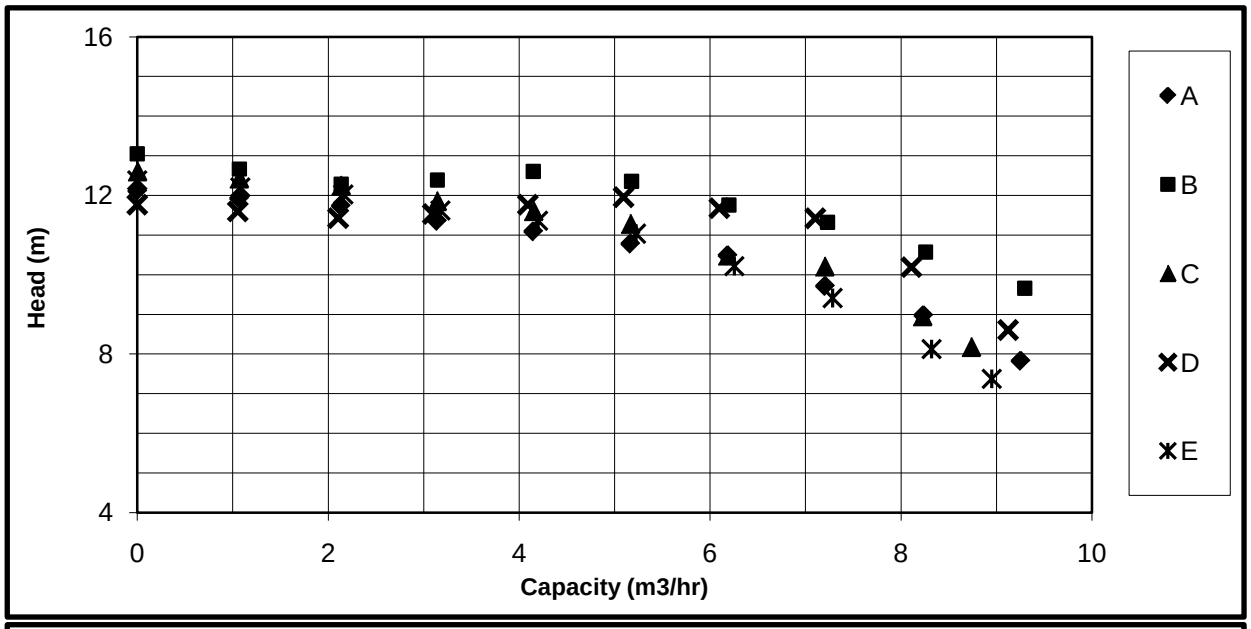

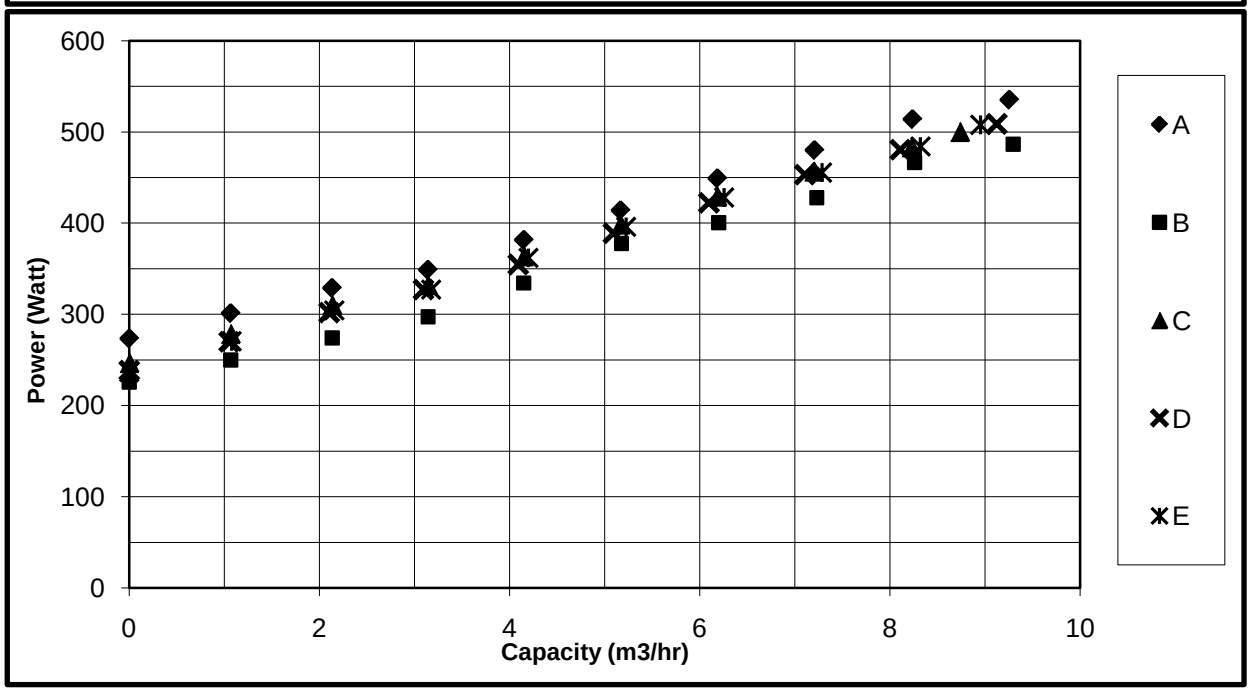

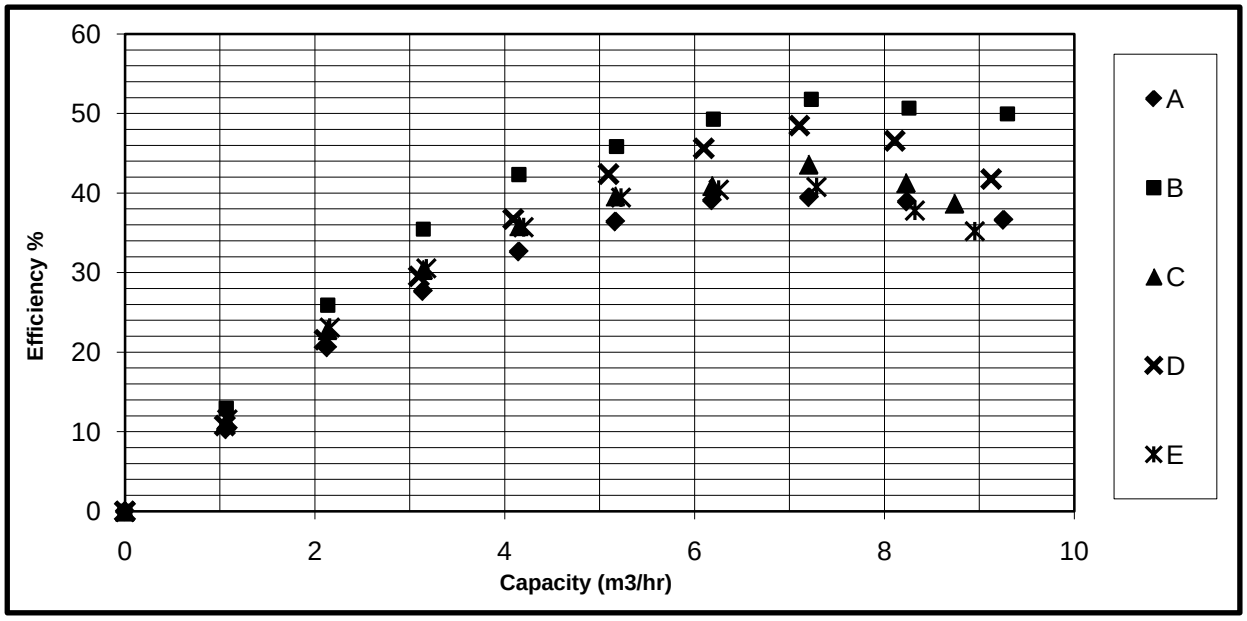

Figure (5-24) Comparison for experimental results for all impeller configurations at 1750 RPM

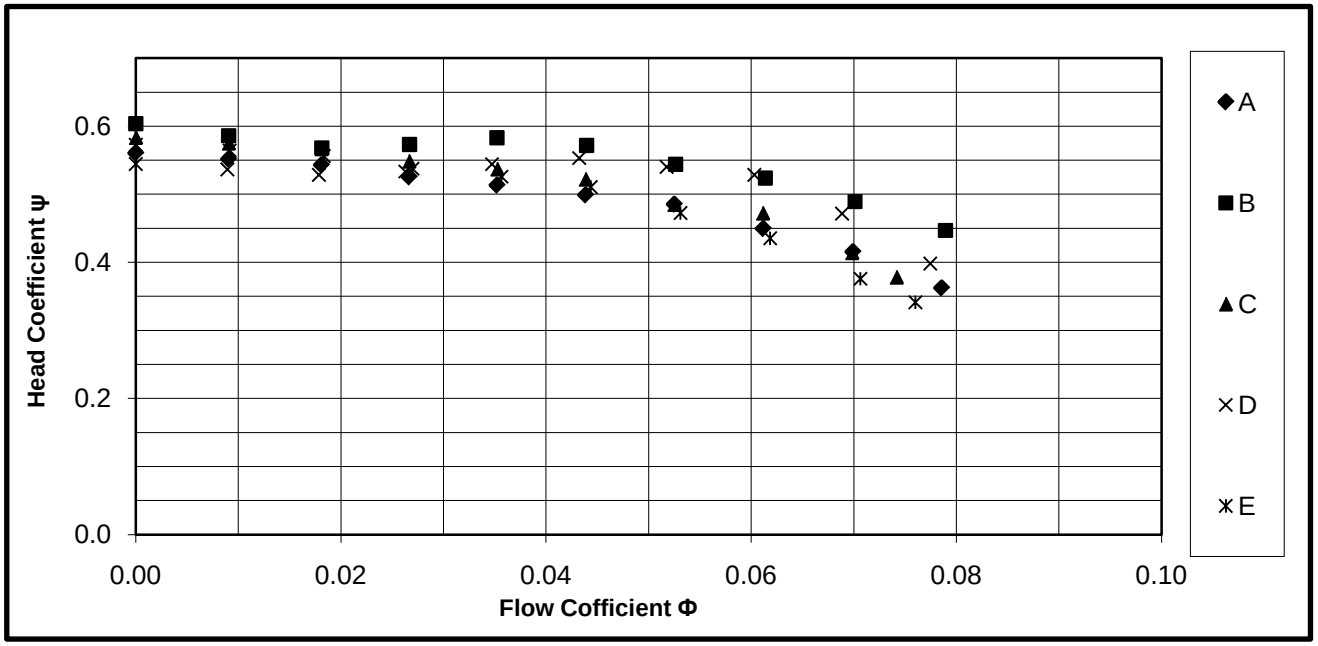

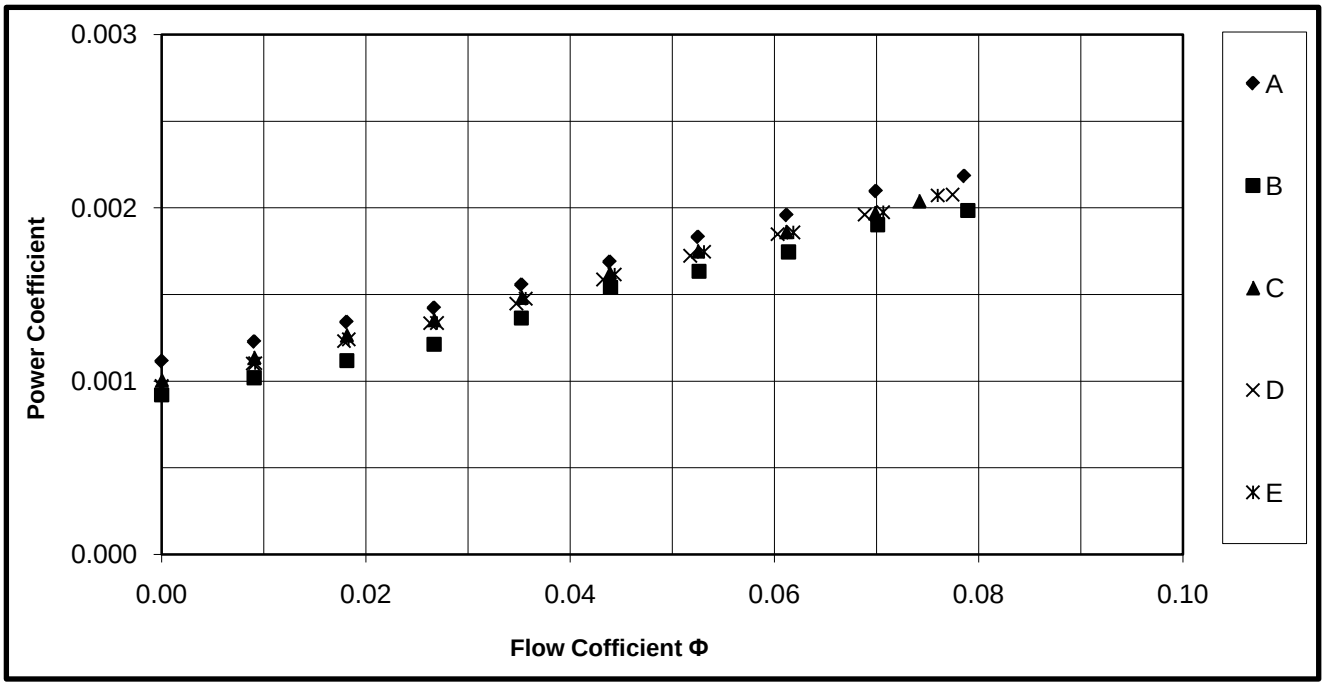

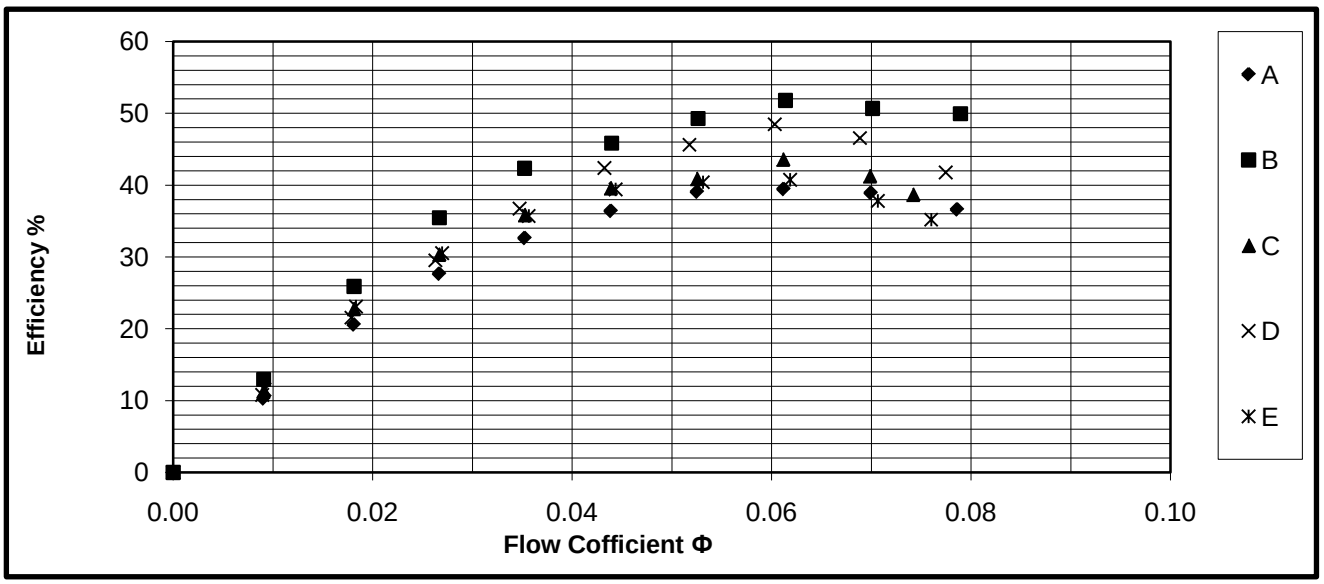

Figure (5-25) Experimental Dimensionless coefficients all impeller configurations at 1750 RPM